

Shatter cones: Branched, rapid fractures formed by shock impact

Amir Sagy

Institute of Earth Sciences, Hebrew University of Jerusalem, Jerusalem, Israel

Jay Fineberg

Racah Institute of Physics, Hebrew University of Jerusalem, Jerusalem, Israel

Ze'ev Reches

Institute of Earth Sciences, Hebrew University of Jerusalem, Jerusalem, Israel

Received 9 February 2004; revised 13 June 2004; accepted 16 July 2004; published 26 October 2004.

[1] Shatter cones are rock discontinuities known only from sites of extraterrestrial impacts, and they are assumed to be formed by impact-induced shock waves. Here we characterize the structure of shatter cones by field and microanalyses and explain their formation by dynamic fracture mechanics. Our analyses reveal that shatter cones always occur as multilevel, three-dimensional networks, 0.01–100 m in size, with hierarchal branched fractures. A typical, individual shatter cone is a curved, oblate branch that bifurcates from its parent fracture (e.g., a larger shatter cone) and expands to form a spoon-like surface. The unique shatter cone striations are arranged in V-shaped pairs whose enclosed angle is constant for a given sample. We propose that shatter cones are the natural consequence of tensile rock fracturing at extreme velocities. First, the structure of shatter cone networks is strikingly similar to the structure of branched networks of experimental dynamic fractures that propagate at high velocities (velocities that approach the Rayleigh wave speed, V_R). Second, “fracture front waves,” generated experimentally by the interaction of a rapidly moving tensile fractures and material inclusions, create tracks on the fracture surface that correspond to the V-shaped striations of shatter cones. Third, applying the front wave concept to our field measurements (Vredefort impact, South Africa) shows that the shatter cones propagated at velocities of 0.98–0.90 V_R , with a systematic velocity decrease from the impact center. These extreme asymptotic velocities require the intense energy flux of impacts. Our model explains all of the structural features of shatter cones (curved surfaces, cone directivity, unique striations, hierarchic, multilevel structure) and their exclusive occurrence at impact sites.

INDEX TERMS: 8010 Structural Geology: Fractures and faults; 8020 Structural Geology: Mechanics; 5420 Planetology: Solid Surface Planets: Impact phenomena (includes cratering); 5104 Physical Properties of Rocks: Fracture and flow; 3944 Mineral Physics: Shock wave experiments; **KEYWORDS:** shatter cones, impact, fracture, dynamic, shock, deformation

Citation: Sagy, A., J. Fineberg, and Z. Reches (2004), Shatter cones: Branched, rapid fractures formed by shock impact, *J. Geophys. Res.*, 109, B10209, doi:10.1029/2004JB003016.

1. Introduction

[2] Shatter cones are rock discontinuities that form in nature during large extraterrestrial impacts. Shatter cones range in size from a few centimeters to a few meters, display curved to conical surfaces decorated with radiating striations, and are best developed in fine grained rocks (Figure 1) [Manton, 1965; Dietz, 1968]. While shatter cones have been analyzed in numerous studies over the last few decades, the central questions related to their formation are still open. In this work, we present a comprehensive analysis of shatter cones that is based on field relations and fracture mechanics

principles, and which explains the unique structural features and formation conditions of shatter cones.

[3] Shatter cones were first described in the Steinheim impact structure and were attributed to a “cryptovolcanic” explosion [Branco and Fraas, 1905]. In a seminal series of works, R. S. Dietz [Dietz, 1947, 1959, 1963; Dietz and Butler, 1964; Dietz, 1967, 1968] argued that shatter cones develop under the “mechanical shock of explosive violence” associated with extraterrestrial impacts. Dietz’s arguments, which were based on the geometry, locations, and spatial orientation of shatter cones, were further supported by the observed directivity of the axes of shatter cones toward a common center at a given site [Hargraves, 1961; Manton, 1965; Howard and Offield, 1968; Stesky and Halls, 1983; Albat, 1988] and by the occurrence of shock metamorphism structures within rocks that contain shatter cones

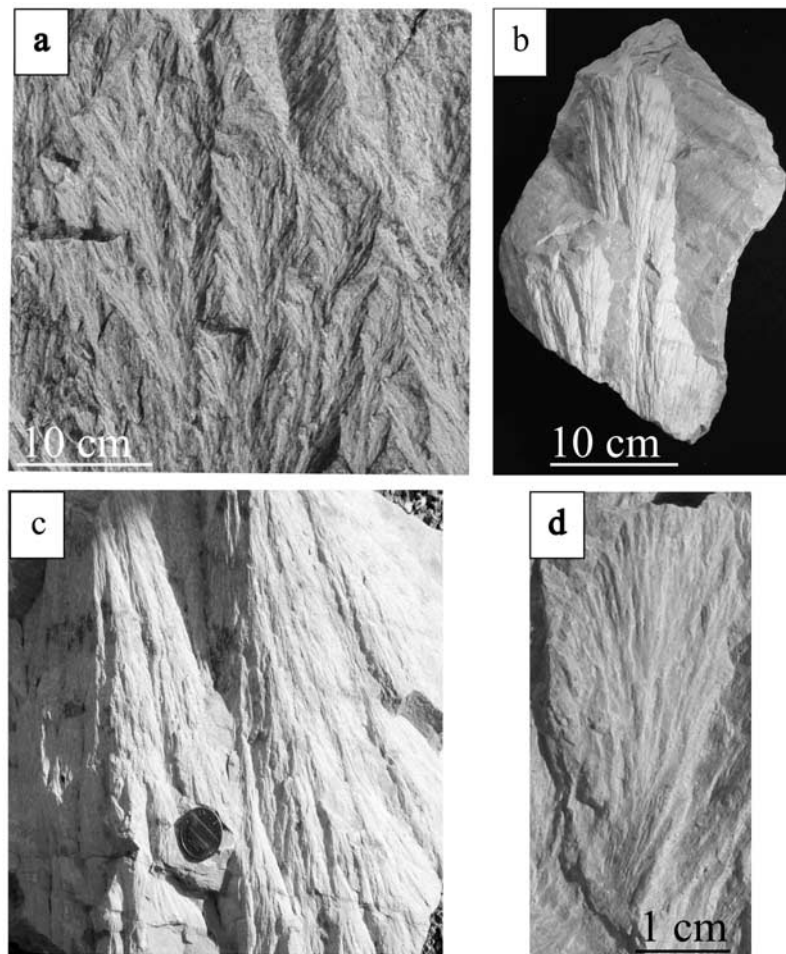


Figure 1. Typical samples of shatter cones. (a) A block of quartzite from Vredefort impact, South Africa, with many small and subparallel shatter cones. (b, c) Dolomite shatter cones from Kentland quarry, Indiana. Note the curved surfaces and the occurrence of several shatter cones in a single hand specimen. (d) Quasi-planar shatter cone in a dolomite sample from Kentland quarry, Indiana. See color version of this figure in the HTML.

[Halls and Grieve, 1976; Reimold et al., 1985]. It is generally accepted that shatter cones are formed by the shock waves propagating within the outer region of the impact zone [French, 1998] and not within the immediate area of the impact where rocks are mostly evaporated, melted, or ejected [Melosh, 1989; O'Keefe and Ahrens, 1993; French, 1998]. Shatter cones were also produced experimentally in high-energy explosions of 5 and 100 t of TNT [Roddy and Davis, 1977], and the stresses needed for shatter cone formation were calculated to be in the 2–6 GPa range. In addition, the impact of high-speed projectiles into limestone samples revealed small, striated surfaces, a few millimeters in size, that strongly resemble shatter cones. These features formed only for impactor velocities exceeding 3 km/s [Schneider and Wagner, 1976].

2. Concepts of Shatter Cone Development

2.1. Previous Analyses

[4] Many field studies showed that shatter cones can be characterized by the following features [e.g., Dietz, 1959; Manton, 1965; Milton, 1977; Albat, 1988; Sharpton et al.,

1996]: (1) Aggregates of shatter cones (horsetail appearance) are common, while complete cones are quite rare; (2) the unique surface striations are the most distinctive property of shatter cones; (3) the apices of most cones point toward the impact center (after retilting of the host rock); and (4) inferred apical angles of shatter cones range over 60° – 120° with $\sim 90^{\circ}$ as a typical value; Nicolaysen and Reimold [1999] later noted that apical angles range up to 180° . It is important to note that early measurements of apical angles were extrapolated from curved surfaces of “partial” cones on the assumption that measured surfaces indeed belonged to complete geometrical cones. The present analysis of shatter cone shapes shows that this assumption is not necessarily correct. Models of shatter cone formation should address these and other features.

[5] Only a few mechanisms have been proposed for the formation of shatter cones. Johnson and Talbot [1964] analyzed shatter cone formation in terms of the interaction between a propagating shock wave and rock heterogeneities. When the impact-generated shock wave progress into a rock mass, the rocks undergoes intense, concentrated deformation across the shock front, and the shock wave

splits into an elastic precursor and delayed plastic wave. When the elastic precursor passes through an inclusion (or heterogeneity), it generates scattered waves, which radiate outward from the inclusion and change the symmetry of the stresses behind the precursor. The model suggests that this process leads to the development of a plastic region with a conical interface that separates the elastic, unperturbed “outer” zone from an “inner,” plastically deformed one. The model proposes that fractures will develop along this conic interface over a narrow range of shock velocities with cone apex angles of 90° , and with cones axes oriented in the direction of the shock source.

[6] In another model, *Gash* [1971] proposed that shatter cones are tensile fractures whose conical geometry is the consequence of the superposition of the main compressive wave at the shock front with waves reflected from free surfaces. This model predicts that shatter cones surfaces will develop parallel to the local principal compressive stresses associated with the interaction of the two waves, and that shatter cones will preferably develop beneath the impact zone. *Baratoux and Melosh* [2003] have recently proposed that shatter cones are conic tensile fractures that develop by constructive interference of the tensional hoop stresses at the tail of the compressive shock wave with tensional scattered waves, which are radiated from inclusions in the rocks.

[7] The above models do not explain a number of central observations, with some observations appearing to contradict their predictions: (1) Field observations of complete cones are very rare [*Manton*, 1965; *Albat and Mayer*, 1989], in contrast to the predicted well-defined conical shape. (2) Observed apical angles of shatter cones vary over quite a large range [*Milton*, 1977] instead of being well-defined 90° angles, and many shatter cones are practically planar surfaces [*Nicolaysen and Reimold*, 1999]. (3) The characteristic striations, which are the most distinctive feature of shatter cones, are not explained by these models.

2.2. Present Approach

[8] Here we present a model for the mechanism of shatter cone formation that is based on new field observations and on recent experimental and theoretical analyses in fracture mechanics. The model provides comprehensive answers to the above open questions and substantiates and expands the concepts introduced by *Sagy et al.* [2002].

[9] It is first hypothesized that shatter cones are tensile fractures and that their unique features reflect the extreme loading conditions generated by large impacts or intense explosions. This extreme loading suggests that shatter cones are highly dynamic (rapid) fractures which propagate at velocities comparable to the Rayleigh wave speed, V_R ; this is the theoretical limiting velocity for tensile fractures [*Freund*, 1990]. To test this hypothesis, we first documented the structure of shatter cones ranging from individual cones to large fractures that are tens of meters in size. We focused on the interrelationship between multiple cones and the fractographic features of individual shatter cones. We then analyzed the morphological features in view of experimental results of rapidly propagating fractures in brittle materials and the corresponding theoretical analyses. Of particular importance are (1) the experimental observations of intrinsic geometric complexity of tensile

fractures which propagate at high velocities [*Sharon et al.*, 1995; *Sharon and Fineberg*, 1996; *Fineberg and Marder*, 1999]; (2) the theoretical analyses [*Ramanathan and Fisher*, 1997; *Morrissey and Rice*, 1998, 2000] and observations of fracture front waves (FW) [*Sharon et al.*, 2001, 2002]; and (3) the experimental evidence [*Ahrens and Rubin*, 1993; *Arakawa et al.*, 2000] and calculations of extreme tensile stresses that develop at the wake of the propagating impact shock front [*Asphaug et al.*, 1996; *Camacho and Ortiz*, 1996; *Baratoux and Melosh*, 2003]. The resulting analysis offers a new picture that links the unique geometry of shatter cones, their orientation, and hierarchic structure to the mechanics of dynamic fracturing.

3. Structure of Shatter Cones

3.1. Field Relations

[10] Our fieldwork was conducted at two areas with an abundance of shatter cones: the Kentland dome, Indiana, and the Vredefort dome in South Africa (Figure 2). The Kentland impact in western Indiana is one of the first sites of shatter cone recognition thanks to the continuous quarrying of the impact dome since the end of the 19th century [*Dietz*, 1947]. The ~ 200 m deep quarry reveals three-dimensional (3-D) exposures of carbonate and sandstone rocks with countless shatter cones. The exposed stratigraphic sequence includes 300 m of Ordovician to Middle Silurian sedimentary rocks that are intensively deformed by large folds and faults [*Gutschick*, 1976, 1983]. Geophysical and structural analyses revealed that the Kentland dome is a circular structure which is about 12 km in external diameter, with a 3–4 km wide central uplift of over 600 m and a depressed outer ring [*Tudor*, 1971; *Laney and Van Schmus*, 1978]. *Dietz* [1947, 1959] suggested that the Kentland dome was generated by an extraterrestrial impact, yet others proposed endogenic explosion origins [*Shrock*, 1937; *Tudor*, 1971]. The impact mechanism is supported by a structural analysis of the exposures and by the existence of shock deformed quartz [*Gutschick*, 1976; *Laney and Van Schmus*, 1978]. The precise impact timing is unknown.

[11] The Vredefort dome is a huge circular structure centered about 120 km southwest of Johannesburg, South Africa (Figure 2b). It includes an inner core of Achaean gneiss with pseudotachylite and an outer collar of sedimentary and volcanic rocks [*Reimold and Gibson*, 1996]. The dominant deformation features of the collar are thrusts and concentric folds, and the estimated dimensions of the deformed zone attributed to the Vredefort dome range from 100 to 300 km in diameter [*Grieve and Pesonen*, 1992; *Therriault et al.*, 1997; *Henkel and Reimold*, 1998]. The lunar geometry of the site and the widespread occurrence of shock induced features (shatter cones, planar deformation features, and high-pressure polymorphs) indicate the extraterrestrial impact origin [*Hargraves*, 1961; *Manton*, 1965; *Dietz*, 1968; *Martini*, 1978], which was dated to 2023 ± 4 Ma [*Kamo et al.*, 1996]. Numerical simulation suggests that the dimensions and deformation of the Vredefort dome are compatible with the impact of a body, 10 km in diameter, having an impact velocity of 20 km/s [*Turtle and Pierazzo*, 1998]. The Vredefort impact site contains

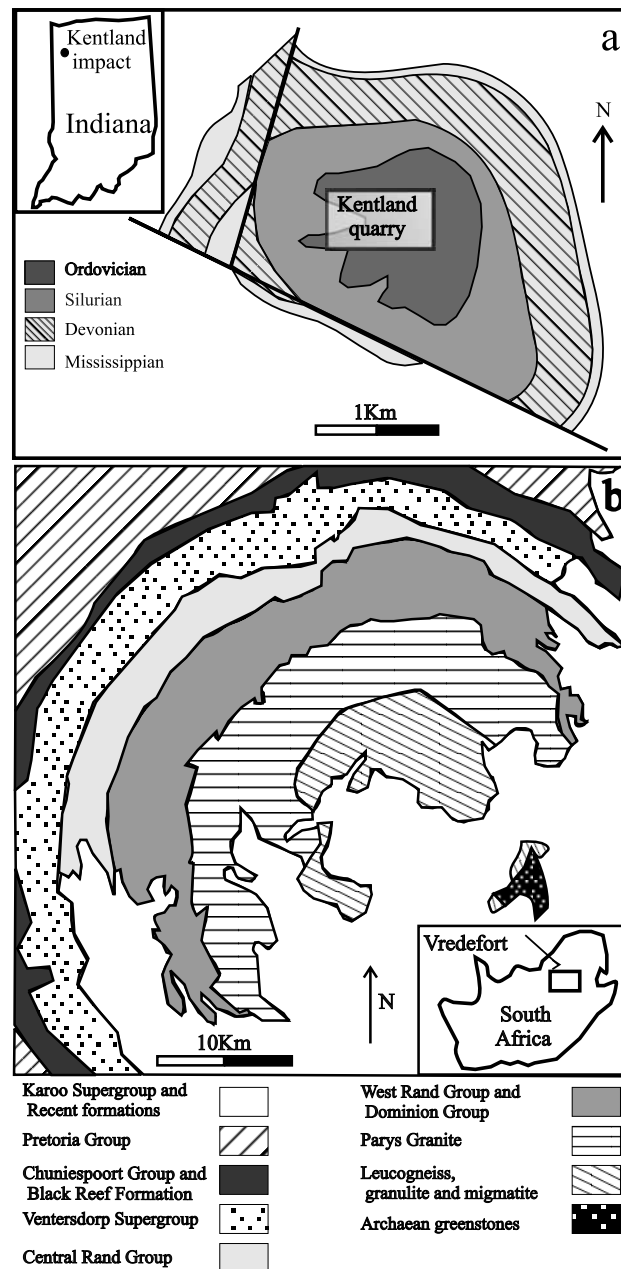


Figure 2. Geologic maps of the studied impact sites. (a) Simplified geologic map of the Kentland impact site, Indiana, with the marked location of the quarry. Modified after *Gutschick* [1983]. (b) Simplified geologic map of the Vredefort impact site, South Africa. Modified after *Bisschoff and Mayer* [1999].

numerous, extensive and diverse exposures of shatter cones in a variety of rock types that are mostly distributed at distances of 15–50 km from the impact center in the northwestern part of the structure [*Therriault et al.*, 1997].

3.2. The Shape of a Single Shatter Cone: Conical or Not?

[12] We examined hundreds of shatter cones that range in size from a few centimeters to a few meters, and which developed in dolomite, limestone and sandstone (in the Kentland quarry) as well as granite, quartzite, slates, chert, and andesites (in the Vredefort dome). One striking feature is, as previously noted by *Manton* [1965], that complete,

whole cones are very rare. Shatter cones appear primarily as clusters of portions of quasi-conical structures that are positioned either on curved surfaces (Figures 1a and 1b) or form complex 3-D bodies. These quasi-conical structures may be divided into three general categories: (1) quasi-planar surfaces (Figure 1d) (also noted by *Nicolaysen and Reimold* [1999]); (2) elliptical cone surfaces (Figure 1c); and (3) elliptical paraboloid/hyperboloid surfaces (Figures 1b and 1a). Details of these shapes are presented below.

[13] The geometry of a single shatter cone is determined here for a typical quasi-conical structure that can be isolated from its neighbors within a cluster (marked in Figure 3). The shape was measured with an optical profilometer that

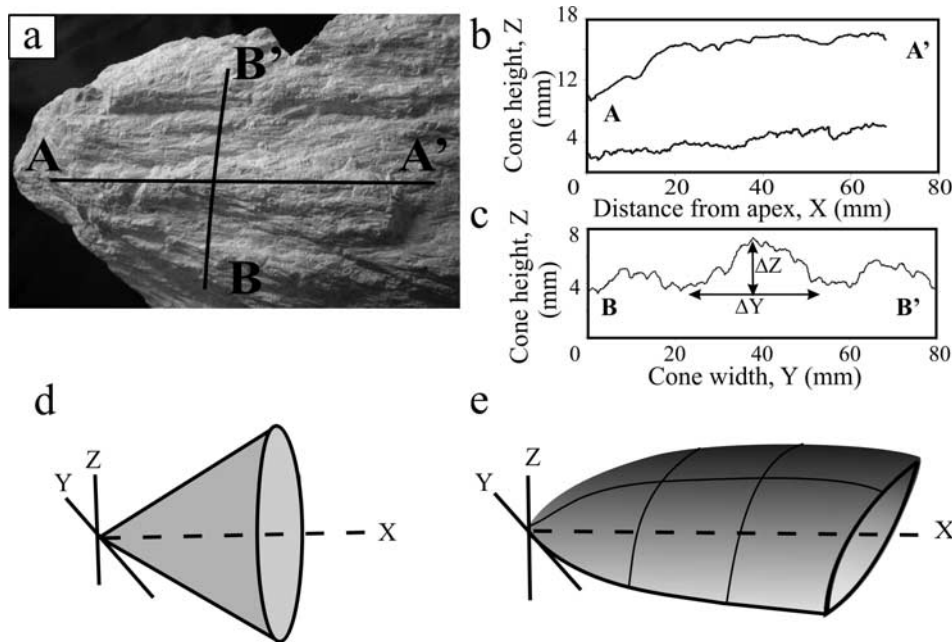


Figure 3. The structure of a single shatter cone. (a) A typical dolomite shatter cone from Kentland impact. Lines A-A' and B-B' mark the locations of topographic scan lines along the shatter cone surface performed with an optical profilometer (see text). (b) Two profilometer scan lines parallel to the direction of the structure axis (A-A') measured on two different shatter cone samples. The short-wavelength roughness is related to the shatter cone striations (see text). At larger scales, the lower profile is quasi-linear, which is consistent with a cone-like shape, whereas the upper profile (A-A' in Figure 3a) has a curved, parabolic shape that does not fit a simple cone geometry. (c) A scan line perpendicular to the axis (B-B' in Figure 3a). Two wavelengths are apparent: a short wavelength (2–3 mm) due to shatter cone striations and long wavelengths (30–40 mm) that describe the surfaces of two or three distinct smaller shatter cones. The relatively small height/width ratio ($\Delta Z/\Delta Y \sim 1:10$) indicates that these small shatter cones have the overall shape indicated by the sketch in Figure 3e. Note that the vertical scale is 2.5 times the horizontal one. (d) Expected height/width ratio in a perfect cone of 1:2. (e) Typical shatter cones observed in our work, which have a much smaller height/width ratio. See color version of this figure in the HTML.

scans 2-D profiles along selected surfaces. We used a laser-based profilometer (Optimet Conoscan 2000) with vertical resolution (Z axis, normal to the measured surface) that ranges from 1 to 10 μm , and with a horizontal stepping (X, Y axis resolution) as fine as 1 μm . Examples of these scanned profiles are A-A' and B-B' in Figure 3a that are, respectively, parallel (X direction) and normal (Y direction) to the shatter cone axis. Figure 3b displays the A-A' profiles of two different samples. The profiles initiate at the apex of each cone, at $X = 0$, and continue along the X direction. The roughness in the two profiles reflects the surface striations (analyzed in section 4). The two measured profiles show that these shatter cones are not necessary conical: the lower profile has a linear, constant slope that is consistent with the profile of a cone (Figure 3d), whereas the upper profile (A-A' in Figure 3a) has a curved, more typical, profile. We found that the exterior, striated surfaces of shatter cones may be convex outward, concave outward, or planar (Figure 1).

[14] Figure 3c displays the B-B' profile (marked in Figure 3a) that is perpendicular to the axis of the shatter cone; this is a Y - Z plot in the cone coordinate system. This profile displays at least two apparent roughness scales: the 2–3 mm waves that reflect the shatter cone striations, which

also appear in Figure 3b (along the cone) and the structures at 30–40 mm scales that correspond to small-scale, secondary cones that are imbedded upon the host cone. These secondary cones are relatively flat as indicated by their small height/width ratios of 1:10 to 1:15 ($\Delta Z/\Delta Y$ in Figure 3c). The overall B-B' profile of Figure 3b is flat when the above roughness is ignored. It is significant to note that these cone profiles are inconsistent with cross sections of a cone as sketched in Figure 3d. The overall profile in Figure 3c is far from the circular cross section that would be expected in a “true” conic profile, as depicted in Figure 3d. One could argue that over a scale of a few meters this curve would indeed inscribe a circle. Yet, in our field observations over many scales, we have hardly observed shatter cones that approach a “complete” closed cone.

[15] These relations of small quasi-conical surfaces that overlap and bound each other are the dominantly observed relations in our extensive examination of shatter cones. The rarity of complete “geometric” cones (at any scale) and the prevalent flat geometry of the observed “cones” (the small height/width ratios as shown in Figure 3e) lead to the conclusion that shatter cones are intrinsically not conical. We find that shatter cones are best described as curved, oblate, spoon-like surfaces with characteristic striations,

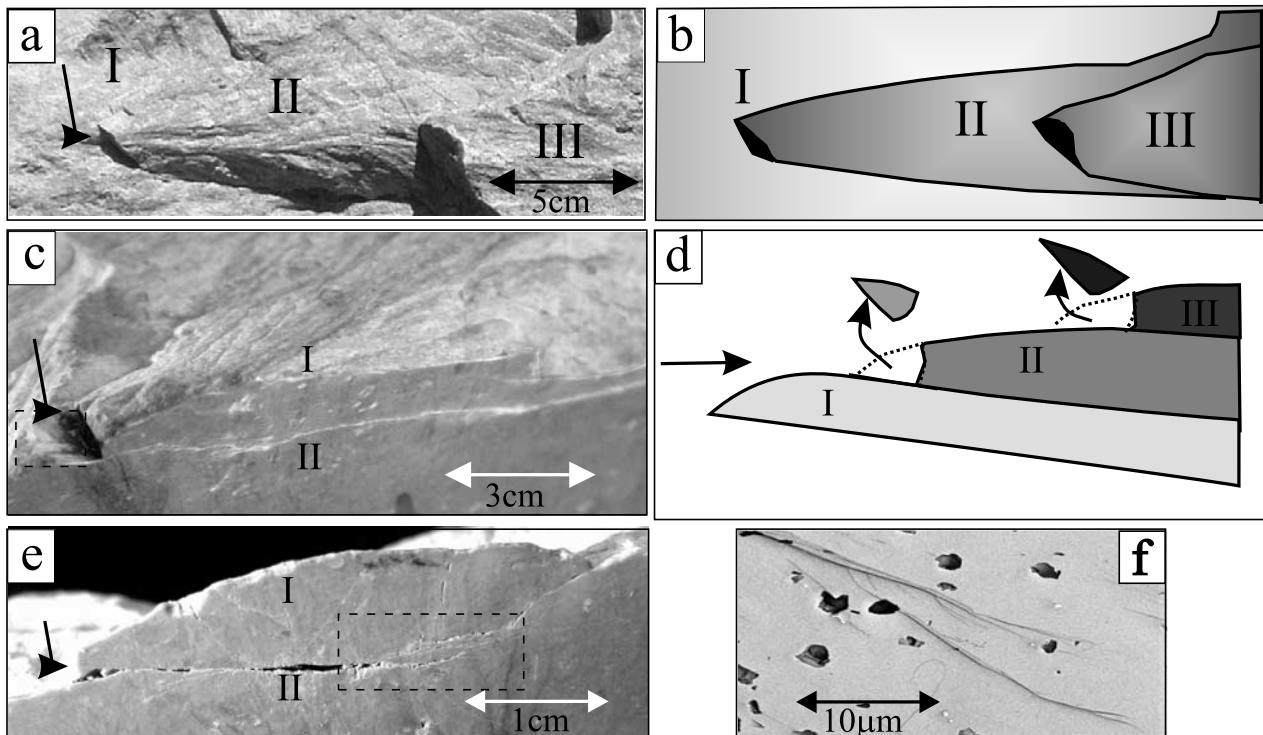


Figure 4. The external and internal structure of shatter cones in dolomite samples from Kentland quarry. (a) Photograph and (b) schematic map of a surface with three aligned shatter cones (marked I, II, and III) in hierarchic, cone-on-cone order. (c) Three-dimensional view of a shatter cone. A front sawcut reveals an internal surface, marked II, that branched away from the upper, external surface, marked I. The branching point is marked by an arrow and the branched surface has a characteristic spoon-like shape. The internal surface II is striated in the same direction as I (framed), and the two surfaces become nearly parallel a few centimeters from the branching point. The dotted lines delineate the cone tip, which commonly breaks off exposed samples. The overall structure explains 3-D horsetail structures. (d) A schematic cross section describing the internal structure of Figures 4a, 4b, and 4c. (e) A shatter cone cross section displaying a spoon-like branch which bifurcated from a point (arrow) on its parent surface. Further branching (framed) occurs from II to generate an additional spoon-like branch with a similar shape. Note the inverse curvature direction of branched surfaces; I is convex downward and II is concave upward (see text). (f) SEM image displaying multiple branching at micron scales. Note that cone tips are preserved in the internal branches presented in both Figures 4e and 4f. See color version of this figure in the HTML.

whose overall shape is described by the sketch in Figure 3e. This description is further supported in section 3.3 by additional observations over several size orders.

[16] We retain the term “shatter cones” for its historical and widespread usage, even though this term does not necessarily imply that the structures are conical. We will use the term “cone axis” to denote the symmetry axis of the shatter cone (X axis in Figures 3d and 3e). The apical angle determined by plotting the striation orientations measured on several partial cones [e.g., Dietz, 1968] is a good indicator of the orientation of the cone axis; however, the value of this angle is a poor representation of the actual shape of the striated surface (as was noted by Nicolaysen and Reimold [1999]).

3.3. Aggregates of Multiple Shatter Cones

3.3.1. Horsetail Structures: Multiscale Networks of Fractures

[17] The most common appearance of shatter cones are in aggregates of multiple, cone-on-cone striated surfaces that

are well known as “horsetail” structures (Figures 1a and 4) [Dietz, 1968; French, 1998]. The cones in the horsetail aggregates overlap each other, and usually their axes are aligned in a single direction (Figure 1). The cones display a hierarchic order with multiple levels of “offspring” cones that are positioned on the surface of larger, “parent” cones. A simple example of this hierarchic order is the succession of three cone structures displayed in Figures 4a and 4b (marked I–III). These cones form a staircase structure in which each offspring cone lies on top of its parent, with the apices of each successive secondary cone aligned roughly along a single line while progressively shifted in the cone axis direction. The multiscale nature of shatter cones is further demonstrated by their internal branched structure displayed in Figures 4c–4e and Figure 5. Particularly significant are the relationships between the external surfaces of the shatter cone (or horsetail structure) and the internal fractures within the same specimen. We examine these relations for a dolomitic shatter cone from Kentland (Figure 5a). The external, striated surface (marked I_1 in

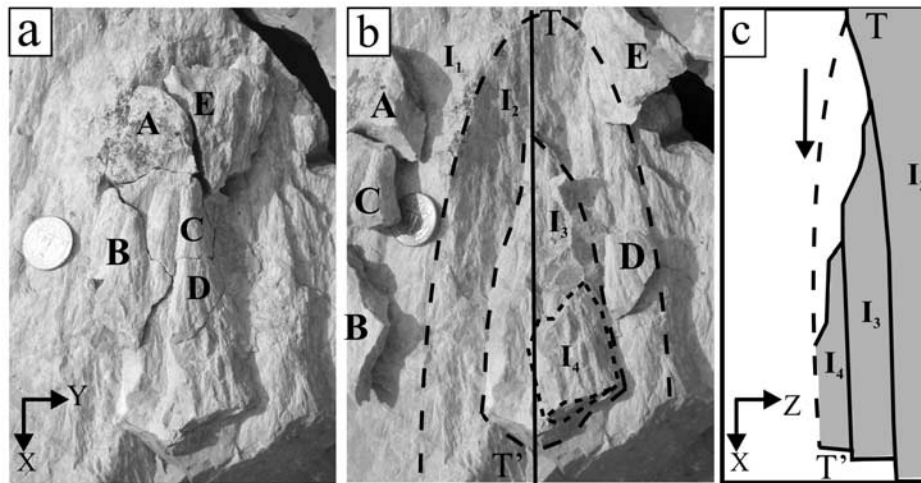


Figure 5. Spoon-like branches in a dolomite sample from Kentland quarry. (a) External surface broken into five fragments (labeled A–E). (b) Same as Figure 5a, but with fragments A–E removed to expose three curved internal branches with striated surfaces. The external parent surface (marked I_1) branches into a series of internal, striated surfaces marked I_2 , I_3 , and I_4 and outlined by dashed lines. I_4 eventually remerges with the parent branch I_1 , as shown in the cross section drawn in Figure 5c along the line T–T' marked in Figure 5b. (c) Cross section. The arrow notes the inferred propagation direction.

Figure 5b) of this sample was peeled off by breaking several pieces (labeled A–E in Figure 5b) and exposing the internal fractures. A few features can be noted.

[18] First, clear shatter cone striations are visible on the internal fractures (Figure 5b), and they are in the same direction as the striations on the external surface; similar striation relations are visible in the specimen of Figure 4c. As the striations are the most distinctive feature of shatter cones (above), we conclude that shatter cone fracturing is penetrative and pervasive inside the rock body. Second, the sense of curvature on the shatter cone surface may differ between the external and internal surfaces. For example, the external surface in Figure 5a is convex upward, which corresponds to outward convexity in this shatter cone block (the common case for shatter cones). However, the large internal surface (marked I_2 in Figure 5b) is concave upward; again, similar relations appear in Figure 4c. This inversion of sense of convexity indicates that the internal fracture surface has a curved, spoon-like geometry, as in Figure 3e for a single shatter cone surface. Third, the branches in many samples became parallel to each other a short distance after the branching point (e.g., Figure 4c). This nearly parallel propagation explains the appearance of parallel subplanar surfaces by Nicolaysen and Reimold [1999].

[19] An additional important point, demonstrated in Figure 5, is the development of multilevel shatter cone surfaces inside the shatter cone. The large concave striated internal surface that we discussed above (I_2 in Figure 5b) includes a number of additional, smaller striated surfaces that are marked I_3 – I_4 in Figure 5b. The curvature of these smaller surfaces, I_3 – I_4 , is opposite in sense to the I_2 surface, namely, similar in sense to the external, parent surface (I_1 in Figure 5b). We interpret these new surfaces as tertiary shatter cones that were created by further branching of the

secondary shatter cone surface, I_2 , with the inverted convexity. The three-dimensional geometry of above sample is summarized in a cross section T–T' along the cone axis in Figure 5c. The curved form of each of these surfaces suggests that each surface is a spoon-like branched fracture of the “preceding” surface; with I_1 as the parent surface, I_2 as the second offspring, I_3 – I_4 as tertiary offspring, and so on.

[20] The geometry of shatter cones can now be understood as the intrinsic 3-D structure that is a product of multilevel branching, where each offspring branch will have a spoon-like, nonconical form. The basic cross section of a shatter cone is more elliptic than conic. The basic geometry of each branch is sketched in Figure 3e, where (as noted in section 3.2) the shatter cones are relatively flat with small height/width ratio ($\Delta Z/\Delta Y$ in Figure 3c). We found that essentially all shatter cone surfaces display such hierarchic multiscale branching, as manifested by the cone-on-cone structure described in Figures 4 and 5. In some cases, we have mapped at least five generations of offspring cones in which striated surfaces are observed to branch off from points on the parent surface.

3.3.2. Shatter Cone Aggregates as Branched Tensile Fractures

[21] The following features indicate that the observed networks of branching shatter cone fractures were formed in tensile mode: (1) The characteristic striations display diverging pairs of grooves (Figure 1) that are geometrically inconsistent with fracture-parallel shear. In the field, we found no evidence of detectable slip. (2) In the majority of the samples examined at scales down to 100 μm , there are no measurable shear displacements (larger than a few millimeters) along the internal fractures (Figure 4f). (3) The appearance of a thin melting coating along surfaces [Gay, 1976; Gibson *et al.*, 1998; Nicolaysen and Reimold, 1999]

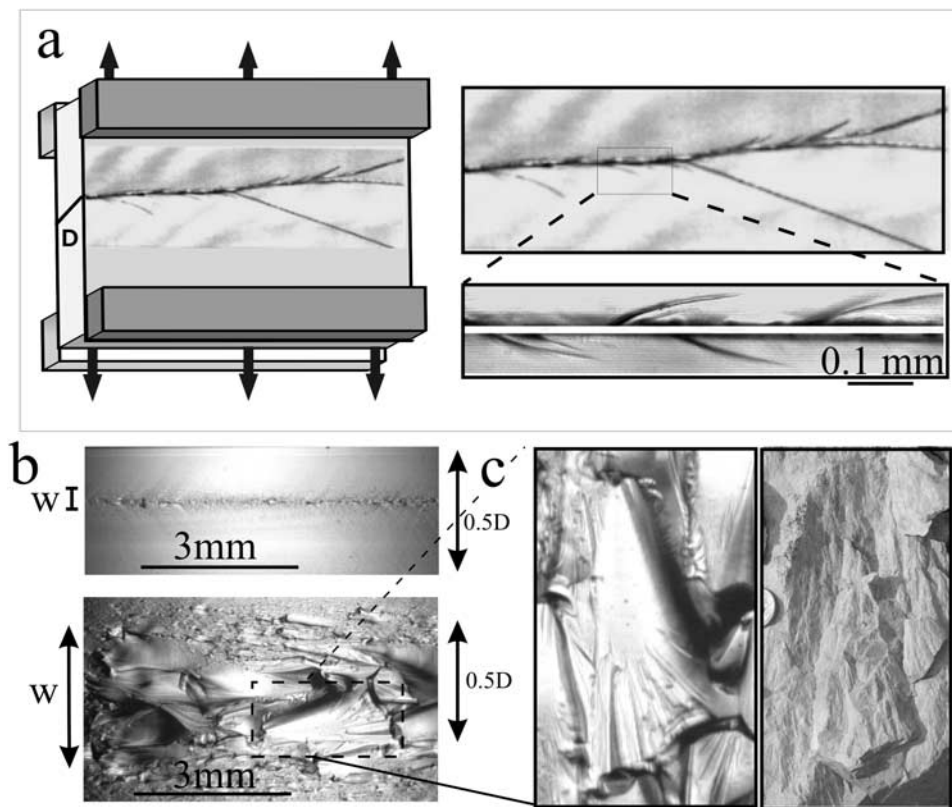


Figure 6. Branching morphology of dynamic tensile fractures in laboratory experiments. (a, left) Schematic view of experimental setting where uniform tension (mode I) is imposed on a glass plate of thickness D (as by Sharon *et al.* [1995], Sharon and Fineberg [1996], and Sagy *et al.* [2001]). (a, right) A typical dynamic fracture generated by this setup (top). The fracture that propagated from left to right at about $0.5V_R$, displays multiscale branching with both large-scale branches and microscopic, microbranches (right bottom). The microbranches have typical curved profiles [Sharon *et al.*, 1995] and width, $W < D$, and they resemble shatter cone cross sections (Figures 4e and 5b). (b) Surface view of a dynamic fracture formed in pure tension in glass. The initiation points of the microbranches (top) are aligned along well-defined zones within the glass plate. As the fracture velocities increase, the initial width, $W \ll D$, of the microbranches increases (bottom) to $W \sim D$, prior to large-scale branching. (c) (left) Close up view of Figure 6b showing details of microbranch 3-D structure, which displays a spoon-like shape similar to (right) typical shatter cone surface.

could be a direct result of rapid tensile fracture in brittle materials [Fuller *et al.*, 1975], and not necessarily indicator of sliding induced melting.

[22] We observed a few cases of shear displacements of up to 1 mm along branches that deviate in orientation from the main shatter cone surface, but these are associated with highly fragmented zones. Since shear displacements above this scale are quite rare, we conclude that shatter cones are tensile fractures and any localized shear probably occurs after the initial tensile fracturing, possibly due to relaxation of shock stresses.

[23] The predominant observed structure of hierarchal branched shatter cone surfaces (Figures 4 and 5 and corresponding text) strongly resembles the structure of dynamic tensile fractures observed in laboratory experiments [Sharon *et al.*, 1995; Sagy *et al.*, 2001], and in the field [Sagy *et al.*, 2001]. Sharon *et al.* [1995] and Sharon and Fineberg [1996] examined the three-dimensional structure of fractures that developed during the propagation of rapid fractures in plates made of glass and brittle

polymers. The plates were loaded under uniform tensile stress (Figure 6a), which lead to the propagation of purely tensile (mode I) fractures. These experiments showed [Sharon *et al.*, 1995] that rapid, dynamic fractures spontaneously spawn both large-scale and small-scale secondary branched fractures or microbranches, when the fracture velocity exceeds 40% of V_R . As demonstrated in Figure 6a, the planar crack symmetry (normal to the propagation direction) is broken by a localized branching event; the initial width of these small-scale microbranches is small compared to the scale of the overall fracture width [Sharon *et al.*, 1995; Sharon and Fineberg, 1996; Fineberg and Marder, 1999]. As shown in Figure 6a (right bottom), microbranches initially branch outward from the propagation direction of the main fracture at angles of $\sim 30^\circ$ [Sharon and Fineberg, 1996] and then curve to propagate approximately parallel to the main fracture. Microbranches are initiated along correlated lines in the propagation direction (Figure 6b, top), display a spoon-like structure and, when sufficiently dense, a cone-on-cone hierarchy (Figure 6b, bottom). As the energy

flux driving the fracture increases, the microbranches increase in both length and width.

[24] The striking similarity between these fractures and the typical form of the shatter cone surfaces (Figures 4d, 4f, and 6c) led us to infer that shatter cones are complex systems of dynamic tensile fractures with the following features:

[25] 1. Shatter cones are curved, spoon-like surfaces with multiscale branching offspring surfaces that are formed by rapid tensile fracturing.

[26] 2. All shatter cones are branched fractures within a multiscale hierarchy. The only difference between small, parasitic cones and larger ones is their scale. This multiscale branching scenario generates the horsetail appearance of shatter cones.

[27] 3. Shatter cone surfaces at all scales retain their typical striations, even within the interior of massive shatter cone blocks.

3.4. Large Fractures That Host Many Shatter Cones

[28] Traditionally, shatter cones have been examined as isolated conical bodies of “hand-specimen” size. Our field observations demonstrate that this view portrays only part of the picture. Here we show that shatter cones are portions of large fractures that display a hierarchic, multiscale pattern of fractures and striations, further expanding the results of the above sections. This is first illustrated by the simple case of Figure 7, which contains many cone-on-cone structures that appear as secondary branches of a larger, meter-sized structure. This meter-sized structure appears as a scaled-up version of the individual hand specimen shatter cones described in the previous section (Figures 1, 4, and 5). Over its entire surface, hierarchal, cone-on-cone structures, similar in many respects to those presented in Figure 4, are evident.

[29] We mapped the shatter cone ensembles that are exposed on large walls in the fine-grain dolostone layers of the Kentland quarry. The mapping focused on five separate, freshly exposed walls that are up to 20 m high, and the mapped areas range from ~ 2 m² to almost 100 m². Four of these walls display face-on views of subvertical, large fractures that are quasi-planar in shape (Figures 8–10), and one wall displays crosscuts of subhorizontal large fractures (Figure 11). The occurrence of both subvertical and subhorizontal large fractures in the quarry reflects the intense folding and faulting associated with the impact that locally rotated the layered rocks. These exposures provide a three-dimensional view of the large fractures.

[30] The dominant feature in the face-on view of the subvertical fractures are tens of patches, 2–20 cm in size, that are decorated with typical shatter cone striations (Figure 8a). These patches vary in shape from quasi-conical, triangular surfaces to planar surfaces that are subparallel in orientation (Figures 8b and 8c). As the shape, size, and striations of these patches are typical for shatter cones, we regard the patches as shatter cone ensembles that are located on a large, quasi-continuous fracture surface. The triangular apices of these cones point in one consistent direction with only minor spatial variations, as shown for the 131 mapped shatter cones on the northern wall (Figure 9). This uniformity in orientation was observed throughout the entire exposure.



Figure 7. (top) Multiple shatter cones in a quartzitic block from Vredefort site (~ 2 m long). Striated surfaces are arranged in a multilevel hierarchy with five marked (1–5) levels. The overall shape of the shatter cone surface is quasi-planar. A close up (bottom) reveals that surface 5 branched out from points on surface 4 (denoted by dashed lines), and surface 4, which is partly broken, reveals the additional striated surface of 3 which lies beneath it. This structure of this block has the hierarchal structure of Figures 4 and 5 but on ~ 10 times larger scale. See color version of this figure in the HTML.

[31] In another exposure, on the western wall, the pattern is slightly different. Here, most of the mapped shatter cones (115 out of 122) point in one direction (horizontal southward), whereas a few shatter cones (7 out of 122) on the same surface point in the antipodal direction (horizontal northward). At one of the sites, the shatter cones radiate away from one central, relatively smooth zone (Figure 10). These two sites probably indicate fractures that propagated away from their initiation points as indicated by the diverging striation directions.

[32] One outstanding exposure in the southern part of the quarry displays a set of subhorizontal fractures in which the main fractures could be traced for distances of tens of meters (Figure 11a). A close-up view reveals that these fractures are composed of many branched segments that split from the main fracture and may eventually rejoin it (Figure 11b). The mean fracture spacing in this exposure is about 0.1 m although at some locations the local

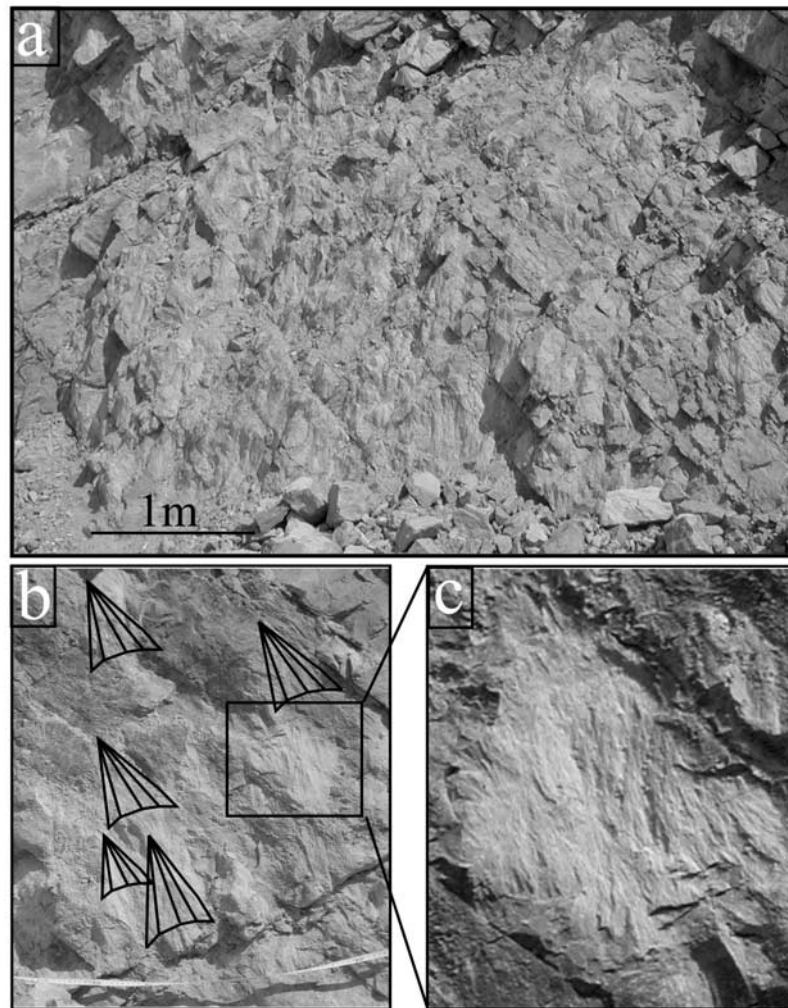


Figure 8. (a) A large, quasi-planar fracture on the northern wall of the Kentland quarry, whose face is decorated by dozens of shatter cones. This fracture intersects several layers without displacing them. We interpret the large-scale roughness of the wall as resulting from branched secondary fractures. (b) Face-on view of an exposure to the right of the exposure presented in Figure 8a, where shatter cones are marked by triangular, cone-like patches. The cone axes and striations of all cones are oriented in a single direction. (c) Close-up view of a single cone. See color version of this figure in the HTML.

fracture spacing decreases to about 1 cm. Here, unlike the exposures of the subvertical fractures of Figures 8–10, the shatter cones striations do not decorate the quarry wall, and they appear only on the surfaces of the subhorizontal fractures (Figures 11c and 11d). Thus the combined observations on both the subvertical and subhorizontal fractures indicate that shatter cones occur exclusively on the large fracture surfaces, in other words, shatter cones are not isolated bodies that are uniformly distributed throughout a massive rock.

[33] These observations indicate that the characteristic features evident on large-scale exposures closely echo the previously described features of the hand specimens: (1) Shatter cones are decorated surfaces found on large fracture surfaces, and they do not occur as isolated structures within a rock body; (2) the large host fractures are most likely tensile in origin as they display no evidence of shear displacement; and (3) the many shatter cones located on the large fractures in the Kentland quarry, on a scale of

1–20 m, strongly resemble, in shape and pattern, the horsetail appearance on a single, small quasi-planar surface (compare Figure 8 with Figure 7). This suggests that a large range of self-similar behavior occurs in the fracturing process.

[34] Finally, the existence of hundreds of oriented shatter cones at scales of dozens of meters suggests that they all belong to a single, coherent fracture surface. The large host tensile fractures spawn many levels of branched fractures, and the shatter cone striations appear solely on these branched surfaces. Our above suggestion that the cones were formed by multiscale branching during the propagation of these main fractures is consistent with the constant directivity of the cone structures within a 100–200 m² size outcrop of parallel fractures (as shown in Figure 11). These observations imply that the large-scale fractures propagated in a preferred direction during the impact in accordance with previous work that suggested a radial propagation direction of shatter cones away from the impact site

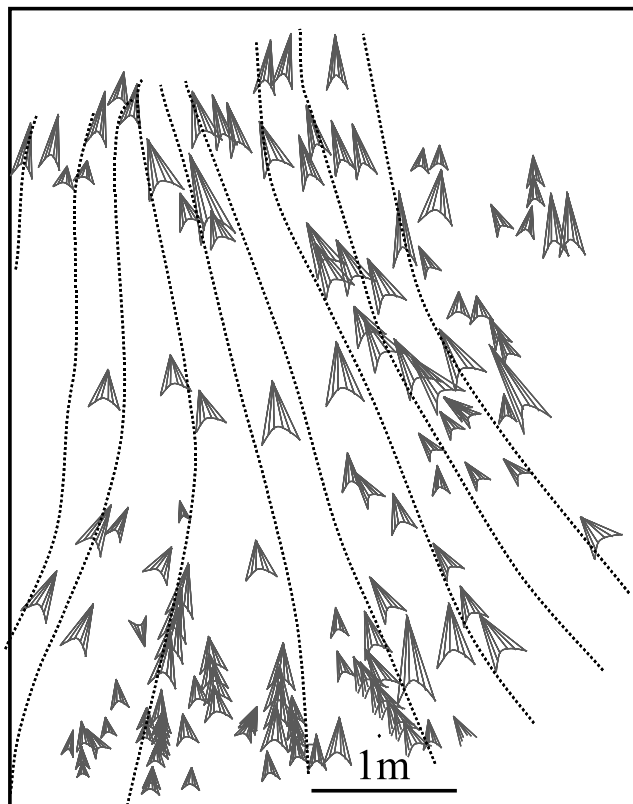


Figure 9. A map of the shatter cones observed on a large fracture on the northern wall of the Kentland quarry (close and subparallel to the fracture of Figure 8a). The fracture face displays an organized pattern of cones (marked by triangular patches) that point upward with small local deviations. As we interpret shatter cones as branched fractures, this coherent directivity of the cone axes suggests they are all part of this large fracture that propagated downward. See color version of this figure in the HTML.

[Hargraves, 1961; Manton, 1965; Howard and Offield, 1968; Stesky and Halls, 1983; Albat, 1988].

4. V Striations: Fractographic Signature of Shatter Cones

4.1. Geometry

4.1.1. General Features

[35] The characteristic striations of shatter cones develop in no other natural structure. As striations appear on all branching surfaces of shatter cones and in a wide range of rock types (Figures 1, 3, 4, and 8), their presence essentially defines the existence of a shatter cone. In spite of the central importance of striations in shatter cone structure, there has been no attempt to explain the mechanism of their formation.

[36] Typical striations are roughly linear in shape, they can be traced for distances up to few centimeters, and their amplitude can reach a few millimeters. The striations display distinct patterns: They generally appear in pairs, and each striation pair diverges from a common vertex point, thereby creating a V-like structure on the shatter cone surface (Figure 12). We define such striation pairs as

“V striations” and the vertex angle enclosed by V striations as the “V angle.” Even by casual inspection, the V striations can be distinguished from slickenside striations on fault surfaces and from the many fractographic features associated with tensile fractures [Bahat, 1991].

[37] Numerous V angles are contained within a given rock sample, which may contain many distinct shatter cones. We measured the distribution of these angles, and to improve the data quality, the analysis is limited to well-preserved samples in which numerous V angles could be unambiguously recognized. V angle distributions of typical shatter cone samples are presented in Figure 12. The V angles in a given sample have a fairly constant value, whereas this value can vary significantly from one sample to another. For example, the mean value of 85 V angles measured in the slate sample of Figure 12a is $21^\circ \pm 4^\circ$, and the mean value of 43 V angles in the quartzite sample (Figure 12b) is $31^\circ \pm 6^\circ$. We also note that the angles are normally distributed about the mean. As we will show in section 4.2, the sharp distributions of the V angles together their measured values are central to our model.

4.1.2. Self-Affinity and the Fractal Dimension of Shatter Cone Striations

[38] Shatter cone surfaces give the visual impression that, even on a single surface, the striations have a wide range of sizes and scales. The scanning electron microscope image (Figure 13) indicates that striations are detectable down to scales comparable to the grain sizes of the sample. This behavior suggests that the shatter cone striations are self-affine, namely, they are statistically self-similar [Roach *et al.*, 1993]. Here we examine the characteristic fractal dimension and self-affinity of these surfaces by using our optical profilometer (see section 3.2) to measure amplitude profiles along shatter cone surfaces.

[39] Feder [1988] defined a self-affine profile as follows. Define $P\{\Delta h(x), \varepsilon\}$ as the probability that a surface height, $h(x)$, has changed by an amount $\Delta h(x)$ within a distance ε from any point x on the surface of the cone. A

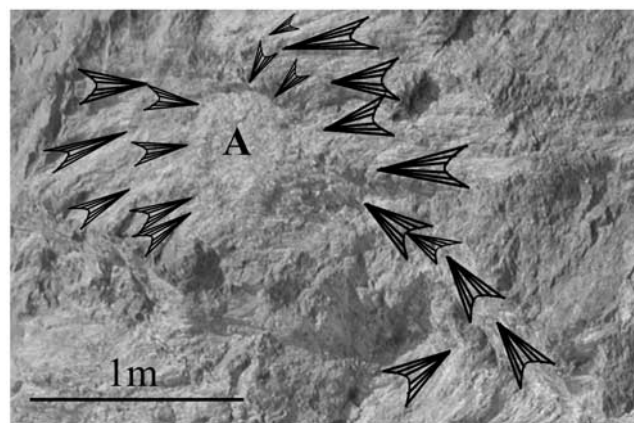


Figure 10. A small portion of the eastern wall at the Kentland quarry that displays shatter cones (marked by triangular patches) radiating away from a central zone. This case suggests that a rapid, radially propagating mode I fracture nucleated at point A. See color version of this figure in the HTML.

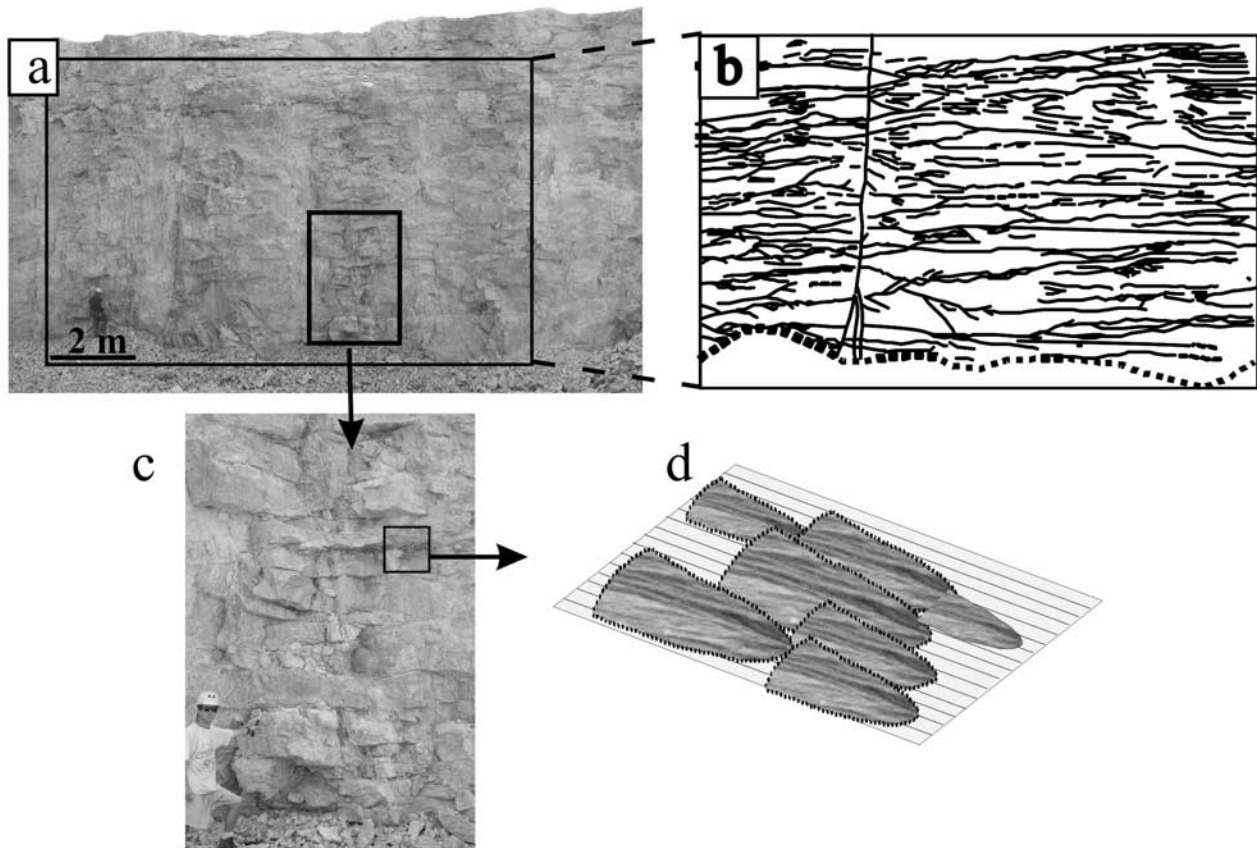


Figure 11. A set of many large, subhorizontal fractures that were crosscut by the southern wall of the Kentland quarry. (a) Photograph and (b) corresponding map of the wall displaying the large fractures. (c) A close-up view showing that many of these fractures are crooked with frequent splits and branches. In this exposure, shatter cones are restricted solely to the surfaces of the large subhorizontal fractures, which are decorated with numerous shatter cones as shown schematically in Figure 11d. Shatter cones are not observed within the rock mass between fractures. See color version of this figure in the HTML.

surface is self-affine if P satisfies the scaling relation [Feder, 1988]

$$P\{\Delta h(x), \varepsilon\} = b^H P\{b^H \Delta h, b\varepsilon\}. \quad (1)$$

In other words, when the length scale is rescaled by a factor b and at the same time we rescale the surface heights by a factor, b^H , then statistically, the surface appears unchanged; namely, P retains the same form up to a multiplicative factor. If relation (1) holds for a given surface, then geometrically, the surface profile has a fractal character and is characterized by a fractal (box counting) dimension of $D = 2 - H$. The box counting dimension (D), is a measure of how, as the scale of the “ruler” (b) decreases, the effective length (L) of the profile increases: $L \sim b^{-D}$. We used the variation method [Dubuc *et al.*, 1989] to quantitatively examine the premise of self-affine behavior and to determine (if the surfaces are indeed self-affine) the fractal dimension, D , of the shatter cone surfaces.

[40] We scanned 20 shatter cone surfaces on five samples (two slate samples and three dolomite samples) and, as a control group, layer and erosive surfaces on the same samples. The scanned areas on the shatter cones were

performed in both the longitudinal (X axis in Figure 14) and transverse (Y axis in Figure 14) directions. Any scanned area includes a matrix of measured points, arranged in 640 distinct scanned lines.

[41] The fractal dimension, D , is calculated for each scan line (Figure 15) by the following procedure which is called the variation method [Dubuc *et al.*, 1989]. We first measure the maximal surface height variation, $v(x, \varepsilon)$ of all surface measurements, within a distance ε (in mm) from every point x along the surface. We then perform the spatial average, $V(\varepsilon) = \langle v(x, \varepsilon) \rangle_x$ over all points x . If a surface is self-affine, the function, $V(\varepsilon)$ will scale with ε as $V(\varepsilon) = \varepsilon^{-H} = \varepsilon^{-(D+2)}$. Where the Hurst exponent, H , is defined in equation (1). The function $\ln(\varepsilon^{-2}V)$ will then be a linear function of $\ln(\varepsilon^{-1})$ with a slope of D (see Figure 15).

[42] In the transverse direction of slate samples, we find a fractal dimension over five scales from 10 μm to 7 mm. In dolomite samples, lines in the transverse direction are self-affine over the range of 10 μm to 1 mm, with a mean fractal dimension of $D = 1.2$. The standard deviation of D is 0.05–0.07 for a given rock sample. The relatively small standard deviation suggests a well-defined fractal geometry for shatter cone striations of a given rock type. For scanned

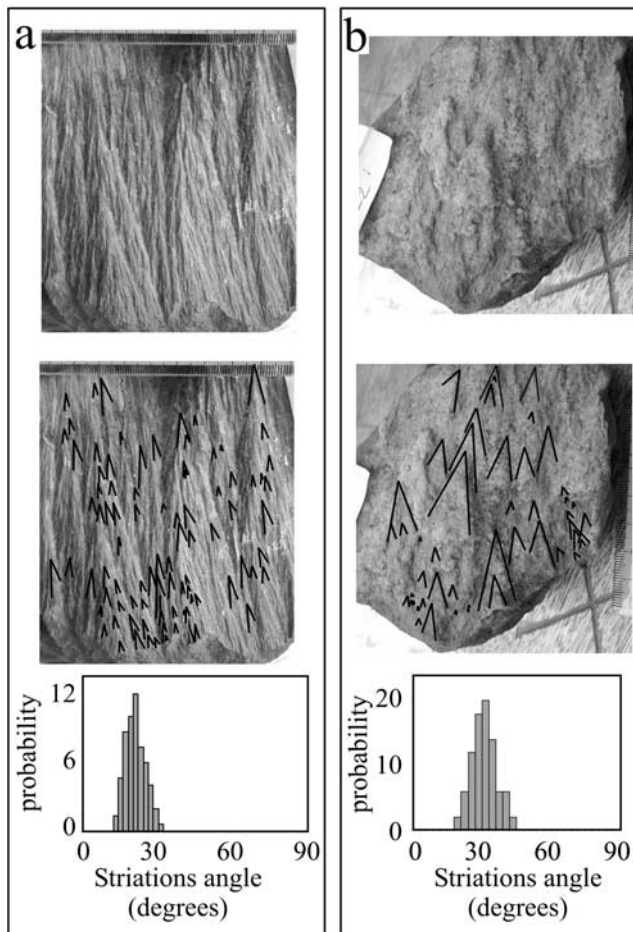


Figure 12. Display of the striations on the surfaces of shatter cones in (a) slate and (b) quartzite from the Vredefort site. The striations are arranged in V-shaped pairs, termed V striations, and enclose a vertex angle termed V angle. (top) Photographs of the respective shatter cone surfaces with (center) marked V angles are presented. (bottom) Histograms showing frequency distributions of the V angles, with mean values of $21^\circ \pm 4^\circ$ (85 measured) and $31^\circ \pm 6^\circ$ (43 measured) for the slate and quartzite samples, respectively. See color version of this figure in the HTML.

lines in the longitudinal direction, the standard deviation of D was much larger (0.1–0.15) with the same mean D . This is possibly due to the fact that in the longitudinal direction fewer striations are sampled, as the scan line is roughly parallel to the striation direction. As Figure 14 indicates, the scaling regime continues down to our measurement resolution. Scattering electron microscope (SEM) images of shatter cone surfaces (Figure 13) indicate that the grain size of the host rock is the lower bound on the width of a striation. Thus the grain size might be the effective lower bound for the self-affine behavior obtained in the profilometer measurements.

[43] We found that the self-affinity changes into a different fractal dimension of 1.45 ± 0.1 at scales larger than a few millimeters for the dolomite samples (Figure 15). The breakdown of the $D = 1.2$ scaling may reflect that, at the larger scales, the measurements range over more than a

single separated branch (i.e., single shatter cone surface). As the self-affine behavior is a measure of the correlated character of a surface, we might not expect the correlations to be retained upon the transition between different (shatter cones) branches (distinct shatter cones). The fractal dimensions calculated for the transverse direction of the shatter cones are consistent with measurements of shatter cones in limestone by *Roach et al.* [1993], where values of 2.24 in 3-D fractal analysis (this value is equivalent to $D = 1.24$ for surface height analysis) were obtained. Our results are also compatible with previous work, which demonstrated a “universal roughness” exponent [*Bouchaud et al.*, 1990; *Hansen et al.*, 1991; *Maloy et al.*, 1992] of surfaces created by tensile fracture in a variety of materials. Finally, we also note that the control measurements of other natural surfaces (layer or erosional surfaces) yielded either inconsistent fractal dimensions or a distinct lack of self-affinity.

[44] In general, the existence of correlations between surface features is a necessary condition for self-affine behavior [*Feder*, 1988]. In particular, if we perform the analysis on a surface that is made up of a number of uncorrelated sections, we will not observe self-affine behavior. In our case, the (nearly 3 orders of magnitude) self-affine behavior that we observe is the result of correlated behavior on a given surface. The above results suggest that striations, at all scales, play a key role in the determination of the fractal nature of shatter cone surfaces. The breakdown of this behavior at large (5–10 mm) scales suggests that a different (or additional) process occurs. It is highly plausible that this process is secondary branching, which (in the measured samples) creates new surfaces at precisely these scales. Thus such surface characterization measurements can distinguish between two distinct types of behavior, secondary branching and striations.

4.2. Mechanism of V Striation Formation

4.2.1. Fracture Front Waves (FW): Experimental Evidence

[45] Our model of V striation formation is based on recent analyses of the effects caused by perturbing the leading edge of a propagating tensile fracture. Theoretical studies [*Ramanathan and Fisher*, 1997; *Morrissey and Rice*, 1998, 2000], and experimental work [*Sharon et al.*, 2001, 2002] have revealed a new type of localized wave, termed a “front wave” (FW), which is excited when a rapidly moving fracture front encounters an inhomogeneity in the material (Figure 16a). It was predicted that FW exist only on the leading edge of a moving fracture front. Recent experiments have shown that a given inhomogeneity will induce a pair of propagating front waves that create a pair of tracks on the fracture surface emanating from inhomogeneity [*Sharon et al.*, 2001, 2002]. The angle, α , enclosed between these tracks follows the relation

$$\cos(\alpha/2) = V/V_{FW}, \quad (2)$$

where V and V_{FW} are the propagation velocities of the fracture front and the FW, respectively (Figure 16) [*Sharon et al.*, 2002]. V_{FW} ranges from $0.96V_R$ to $1.0V_R$. V_R is the Rayleigh wave speed that is the maximal theoretical velocity of tensile fractures propagation. V_{FW} is independent

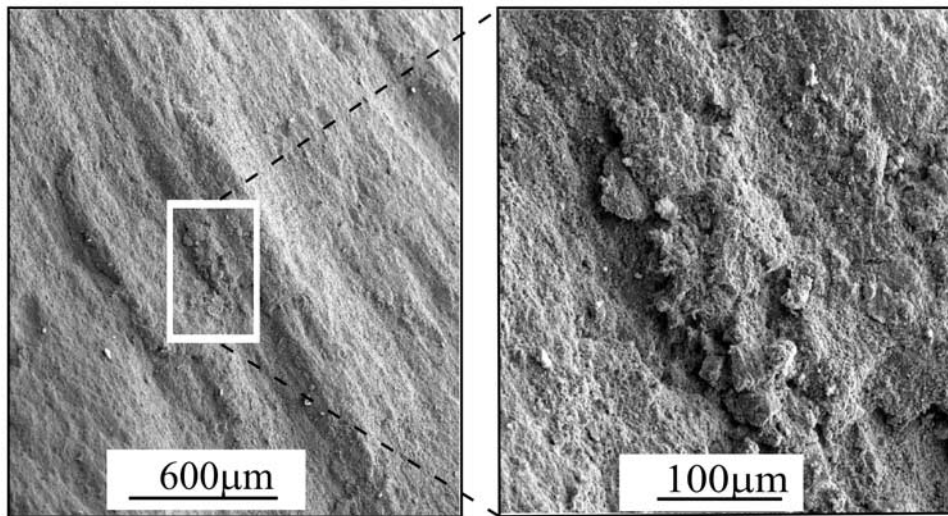


Figure 13. SEM images of the striated surface of a dolomite shatter cone. The striations are observed down to nearly the grain size dimensions.

of both the intensity of the tensile stress driving the fracture and the loading velocity.

4.2.2. Striations as Surface Perturbations Formed by Fracture Front Waves

[46] We now propose that shatter cone striations are the tracks of FW generated by the interaction of the rapidly moving fracture front, which forms a shatter cone surface, with inhomogeneities embedded within the host rock. Thus

the V angles between striations are equivalent to the angle α defined in equation (2) (see Figure 16a). This interpretation of the shatter cone striations is a natural consequence of our hypothesis that shatter cone surfaces are fracture surfaces formed by branched dynamic fractures. Further, this interpretation leads to three predictions: (1) Striations should be observed in V-like pairs; (2) the V angles of shatter cone striations in a given sample should be approximately

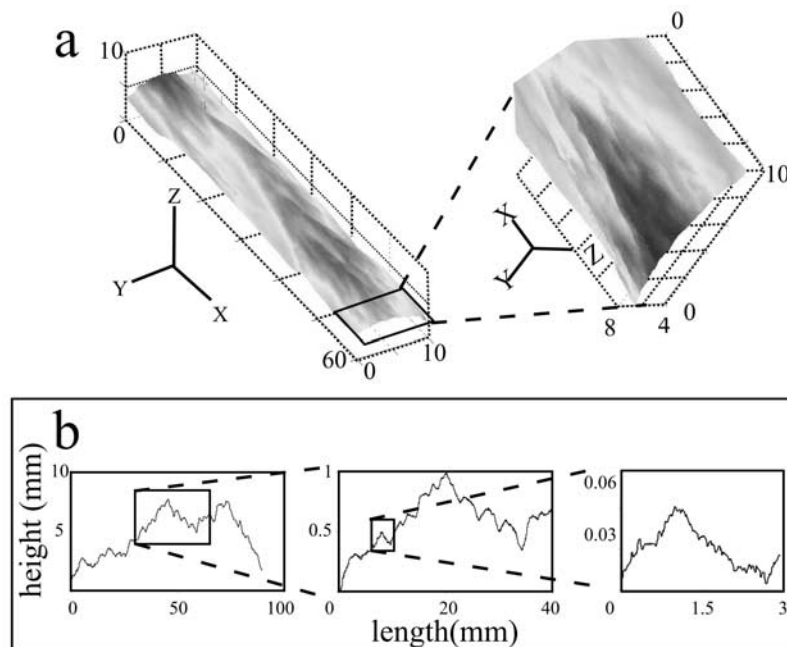


Figure 14. Three-dimensional microtopography of a slate shatter cone surface measured with an optical profilometer (see text). Measurements were performed with 10 μm steps in the Y direction. (a) Topography of a rectangular area (10 mm by 100 mm and enlarges 10 mm by 10 mm on the right), where surface elevations are mapped (dark and bright denote higher and lower elevations). Note the distinct V shape of the striations at several scales. (b) Cross sections in the YZ plane for a shatter cone surface in slate which includes that part of Figure 14a, where the Z axis is expanded. The progressive enlargements shown are indicative of self-affine behavior. See color version of this figure in the HTML.

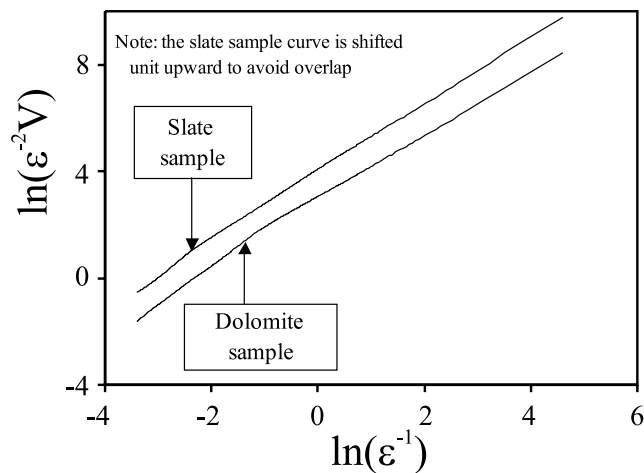


Figure 15. Self-affinity of the striation roughness on shatter cone surfaces. Presented are results of two typical samples with YZ profilometer scan lines (see text). The fractal dimension of a self-affine surface, D , is given by the slope of the graph derived according to the variation method [Dubuc *et al.*, 1989]. If a surface is fractal, the function, $\ln(\varepsilon^{-2}V)$ will be a linear function of $\ln(\varepsilon^{-1})$ with a slope of D (see text). The slate sample (upper curve, shifted by 1 unit to avoid overlap) displays $D = 1.25$ for $10\ \mu\text{m}$ to $7\ \text{mm}$ scale; the $7\ \text{mm}$ limit is indicated by an arrow. The dolomite sample (lower curve) displays $D = 1.15$ for $20\ \mu\text{m}$ to $2.5\ \text{mm}$ scale, and $D = 1.45$ for the $2.5\ \text{mm}$ to $35\ \text{mm}$ scale; an arrow indicates the transition.

constant since the speed of the fracture front remains fairly constant over the centimeter-scale of the sample; and (3) since the driving stress of the fracture process is likely to decrease with the distance, r , from the impact center [Melosh, 1989], the fracture velocity, V , should also decrease with r . Equation (2) thus predicts that α should be an increasing function of r .

4.2.3. Testing of the FW Hypothesis in the Field

[47] We already demonstrated in section 4.1.1 that the first two of the above predictions are satisfied by the surface striations (Figures 12 and 16c). We tested the third prediction by field measurements of the V angles distributed throughout the northwestern part of the Vredefort ring (Figure 2b) [Sagy *et al.*, 2002]. At each site, two to ten samples of shatter cones were collected, including granite, quartzite, slates, chert, and andesites. At least 20 V angles were measured on each sample. To reduce measurement errors, the measurements were restricted to pairs of striations that clearly emanated from well-defined points. The angles were measured manually with a protractor. We were careful to distinguish between the cone apical angles and the angles of the striations, and did not use samples in which the separation between cone and striation angles was not clear. The location of the impact site is estimated with a precision of about two kilometers, and as all samples were collected in the northwestern quarter of the ring (Figure 2b), the measurement error in determining the distance r does not significantly affect our determination of the relative distances between sampling sites. We also note that the area was subject to massive postimpact rearrangement, as well as erosion of about $8\text{--}11\ \text{km}$ [e.g., Gibson *et al.*, 1998]; these

processes could distort our estimates of the distance of the measurement sites from the original impact. The angles in a single sample are normally distributed with standard deviations in the range of $4^\circ\text{--}9^\circ$ (error bars in Figure 17a). The standard deviation is small in samples with many, clear striations. For example, the slate and quartzite samples, with measured 85 and $43\ V$ angles, respectively, have standard deviations of 4° and 6° (Figure 12).

[48] The V angles measurements in the Vredefort impact are displayed by the mean V angles (α) versus the distance r from the impact center (Figure 17a). Also shown the standard deviations (error bars) for the five rock types as they are distributed in the field. The V angles increase systematically with r : the mean values range from $\alpha \sim 20^\circ$ at $r \sim 15\ \text{km}$ to $\alpha \sim 40^\circ$ at $r \sim 40\ \text{km}$. While most samples fall into this range, the quartzite samples display the clearest, systematic angular change, whereas the andesite samples are more scattered. The plot indicates somewhat different angles for different rock types that are located at similar distances from the impact site. For example, the mean V angle in slate samples located at distances of $25\text{--}26\ \text{km}$ is $21.5^\circ \pm 4.5^\circ$ (at two sites), whereas the mean V angle in quartzite samples at a distance of $24\ \text{km}$ is $25.5^\circ \pm 3^\circ$ (three sites).

[49] The systematic increase of the V angles for the five rock types shown is consistent with both the relation between V and α predicted by equation (2) and the reasonable assumption that the fracture propagation velocity decreases with the distance from the impact center. Now we use equation (2) to convert the V angle data to the relative propagation velocity, $V/V_{\text{FW}} \sim V/V_R$ and find that (Figure 17b) the measured values of α ranging from 20° to 45° imply that V/V_R decreases from 0.98 to 0.92 over our measurement range ($15\text{--}40\ \text{km}$ from the impact). Significantly, we see that at the closest point to the impact site, the velocity approaches the limiting value, V_R , for the propagation velocity of tensile fractures.

4.3. Significance of the V Angle Measurements

[50] The velocities indicated by our measurements are significantly larger than the maximal mean velocities of fractures measured in laboratory experiments ($V_{\text{max}} = 0.6\text{--}0.7V_R$) on amorphous noncrystalline materials [Fineberg and Marder, 1999]. Sharon and Fineberg [1996] explained this practical experimental limit on the propagation velocity by the intensification of secondary branched fractures, which form spontaneously above a critical velocity of $V \sim 0.4 V_R$. The fracture energy consumed by this multi-scale branching reduces the mechanical energy available for fracture acceleration. At the time of shatter cone formation, huge energy densities are generated by the impact. The near limiting velocities yielded by our analysis of the V angles, which are not obtainable in laboratory experiments, are an expected consequence of these extreme energy densities.

[51] We can use our measurements of V/V_R to estimate the scaling of these tensile stresses (and hence the pressure field) as function of the distance from the impact center. We derived a simple model (details in Appendix A) that uses the dependence of V/V_R with the distance, r , to evaluate the tensile stress decay at the Vredefort site. It is assumed that the energy density due to the impact-generated shock wave was sufficiently large so that enough energy is encompassed

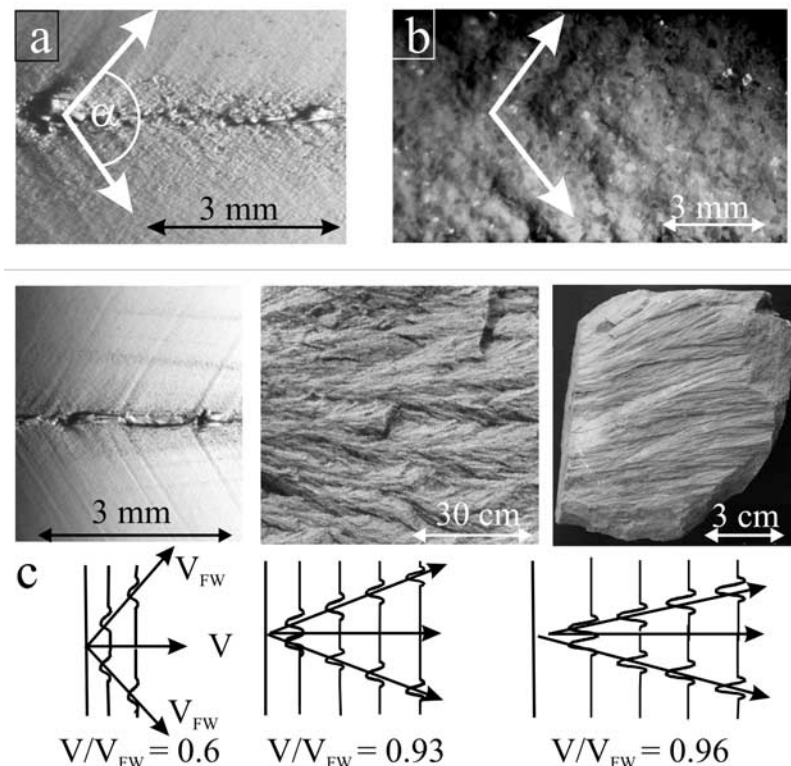


Figure 16. Characteristics of fracture front waves (FW) on the surfaces of rapid tensile fractures. They form when the front of a rapid fracture encounters either an obstacle or upon microbranch formation (see text) [Sharon *et al.*, 2001]. The distinct V-shaped tracks of FW are shown in the fracture surface photographs of (a) glass and (b) artificial rock. All fractures in this figure propagated from left to right in all images. The FW tracks, marked by the two diverging arrows, emanate from their source at an angle α . We identify the V striations of shatter cones with FW tracks [Sagy *et al.*, 2002]. (c) Comparison between the V striations and the experimentally observed FW tracks: (top) FW marks in glass (left) and V striations on quartzite (middle) and slate (right) shatter cones; (bottom) diagrams of FW tracks associated with these samples; each line in the diagram denotes a pair of counterpropagating pulses, propagating along the moving fracture front, at sequential times. The calculated normalized velocities are $V/V_R = 0.6$ (glass), $V/V_R = 0.93$ (quartzite), and $V/V_R = 0.96$ (slate); velocity calculation based of the V angles (see text). See color version of this figure in the HTML.

within the “local” volume of any single crack to drive the fracture process. The equation of motion for a single, rapidly propagating fracture [Freund, 1990] corresponding to this assumption together with an assumed Weibull distribution of initial flaws then predict that the tensile stress, σ , decays with r as $\sigma \propto r^{-\beta}$, where $2.3 < \beta < 3.8$ depends on the value of the Weibull exponent (Appendix A).

[52] Thus, although indirect, our measurements of the V angles provide the first quantitative estimate of the spatial dependence of the tensile stresses generated by large impacts. The model, moreover, has predictive power beyond the specific context for which it was developed.

5. Synthesis: Mechanism of Shatter Cone Formation

[53] The field observations presented here can be summarized as followed:

[54] 1. Shatter cones are spoon-like, curved tensile fractures whose fracture surface is decorated by V striations, their unique fractographic feature.

[55] 2. Shatter cone geometry is generated by 3-D branching of fracture surfaces. They vary in shape from quasi-conical to planar and thus are, in general, inconsistent with models which predict only large apical angles.

[56] 3. Shatter cones form multilevel, 3-D networks of hierarchal branching fractures in the approximate range of 0.01–100 m. The well-known cone-on-cone structures (horsetail structures) are the manifestation of these networks.

[57] 4. The surfaces decorated by V striations display statistically self-similar (self-affine) behavior over their complete range of scales, from 10 μm to almost 10 mm.

[58] 5. The directions of V striation bisectors are all relatively uniform for a given site. This direction is parallel to the propagation direction of the host shatter cone, as commonly accepted.

[59] We interpret these observations in terms of the following experimental and theoretical concepts of fracture mechanics:

[60] 1. The multiscale branching of shatter cones indicates that shatter cones are dynamic fractures, which, as

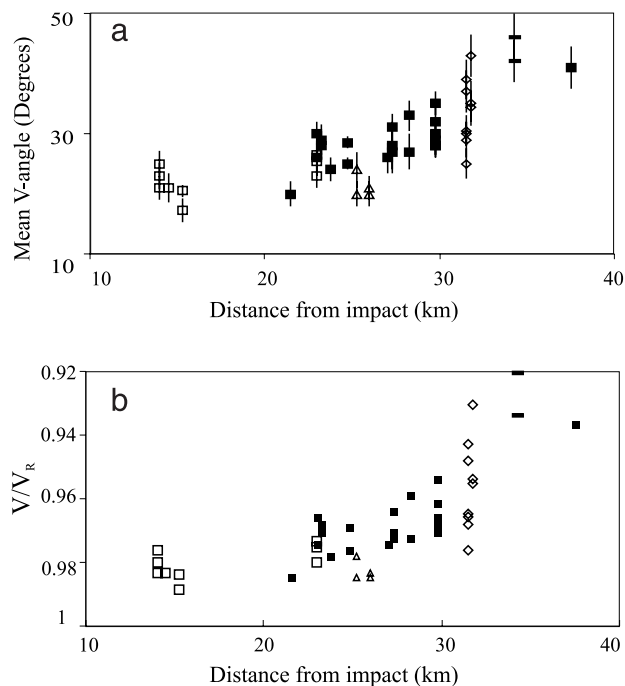


Figure 17. V angles of shatter cone striations (α in Figure 16) measured in Vredefort site (Figure 2), and the associated propagation velocity, V/V_R (see text) (a) Systematic increase of α with distance from the impact center as measured for samples collected at numerous sites, which include granite (open squares), quartzite (solid squares), slates (triangles), andesite (diamonds), and chert (bars). (b) Normalized fracture velocity, V/V_R , versus distance from the impact center in Vredefort. Velocities were calculated by using the relations $V/V_R = \cos(\alpha/2)$, for the mean V angle, α , in Figure 17a [see Sharon et al., 2001; Sagy et al., 2002].

documented in numerous laboratory studies, undergo spontaneous branching at high velocities. The branches increase in size and density as the energy flux, which drives them, increases.

[61] 2. The shape of shatter cones closely resembles that of spoon-like branched fracture surfaces. These evolve spontaneously from a rapidly propagating planar fracture in laboratory experiments of pure mode I (tensile) fracture, when the propagation velocity exceeds $\sim 0.4V_R$. Our field observations (Figures 3–7) suggest that shatter cones are generated in the same fashion. They, however, differ from laboratory experiments in both the large scales of the fractures and fractured media as well as the huge energy scales involved. In general, the dynamics of rapid fractures in a 3-D medium are poorly understood and shatter cones may serve as well-defined examples of this process in nature.

[62] 3. The geometric similarity between V striations on shatter cones and fracture surface perturbations generate by fracture front waves, FW, led us to hypothesize that V striations are natural FW. By applying the theoretical and experiment results to field measurements at the Vredefort impact site, we found that shatter cones propagate at a velocity that is at least $0.90V_R$ and may reach $0.98V_R$. The calculated propagation velocities decrease systematically with distance from the impact site.

[63] On the basis of these observations and interpretations, we proposed that shatter cones form by the following process. As the shock front propagates away from the impact site, a zone of intense tensile stresses develops at its tail [Melosh et al., 1992; Baratoux and Melosh, 2003]. The high-energy density associated with these stresses drives dynamic tensile fractures at extreme velocities of 0.9–0.98 times the theoretical speed limit. The developing fractures could be tens of meters in size, and they are pervasively branched at multiple levels and in three dimensions. These branched fractures, which have a characteristic spoon-like three-dimensional structure, are the observed shatter cones. The unique striations on shatter cone surfaces are formed by the interaction of the fracture front with rock heterogeneities; these V striations are the most reliable indicators of propagation direction and velocity. As these processes require extreme conditions, it is expected that shatter cones will develop only in limited environments, such as large extraterrestrial impact sites.

6. Discussion

[64] The present model differs in several central aspects from previous ones. While here the shatter cones are branched, secondary fractures that bifurcated from a larger coherent fracture, previous models assumed that the basic structural unit of shatter cones is an isolated conic curved structure. Accordingly, these models determine the mechanical conditions for the development of an idealized conical body, and suggested that shatter cones are the product of the interaction between waves scattered from a heterogeneity and the shock pulse [Johnson and Talbot, 1964; Baratoux and Melosh, 2003]. Our model does not exclude such interactions, but we submit that the dominant operating mechanism of the curved branching is the well-known branching instability of dynamic fracturing [Fineberg and Marder, 1999].

[65] Both our model and the model of Baratoux and Melosh assume that shatter cone formation is driven by the tensile stresses that develop in the tail of the shock wave. Baratoux and Melosh [2003] and Melosh et al. [1992] numerically derived the intensity of these stresses for a set of reasonable conditions, and found that these stresses could be as intense as 0.5 of the compressive pressure of the shock front; thus the tensile stresses could exceed a few gigapascals [Baratoux and Melosh, 2003, Figure 1]. Here the two models deviate from each other. As these stresses are very large with respect to rocks tensile strength, it is our view that they are sufficient to cause tensile failure of the host rocks without additional amplification [Vardar and Finnie, 1977; Ahrens and Rubin, 1993]. Baratoux and Melosh, on the other hand, suggested that failure occurs when the mentioned tensile stresses are further amplified by the scattering due to weak heterogeneities. This local stress amplification could be incorporated into our model, serving, for example, as a trigger for branching initiation. In this view, the modified stress field would determine the direction, departure angle, and size of a local branch, where as in the work by Yoffe [1951], a branch will propagate in mode I in a direction normal to the maximal hoop stress. Since most shatter cone surfaces are oblate in shape and do not create a closed, conical geometry,

more detailed, 3-D numerical simulations are needed to link the two models.

[66] In conclusion, once the tensile stresses are large enough to precipitate fracture, many field observations regarding shatter cones can be explained in our model. These include the overall hierarchy of shatter cone structures at scales ranging from hundreds of meters to centimeters, the specific shape of a single cone, and their characteristic striations. No further assumptions, beyond the use of known consequences of dynamic fracture mechanics, are needed.

Appendix A: Tensile Stress Distribution During Impact

[67] While the propagating shock wave induces high compressive pressure at its front, high tensile stresses develop at its tail [Melosh *et al.*, 1992], and according to the present model, these tensile stresses lead to the formation of shatter cones as tensile (mode I) fractures. The formation of tensile fractures under impact conditions has been documented in a number of experimental works [Field, 1971; Evans *et al.*, 1978; Ahrens and Rubin, 1993; Riou *et al.*, 1998; Arakawa *et al.*, 2000]. Additional numerical work has verified both the development of tensile stresses and radially propagating tensile fractures resulting from large impacts [Evans *et al.*, 1978; Asphaug *et al.*, 1996; Camacho and Ortiz, 1996; Repetto *et al.*, 2000; Simha *et al.*, 2002]. Recent work of Baratoux and Melosh [2003] has further demonstrated that shatter cones could result from the tensional hoop stresses found at the tail of a compressive shock front.

[68] We now use the values of V/V_R presented in Figure 17b to estimate the scaling of these tensile stresses (and hence the pressure field) as function of the distance from the impact center at the Vredefort site. We must first correct the current locations of our sampling sites with respect to the impact center, to their respective locations at the time of the impact. The estimated size of the impactor at Vredefort is 10 km in diameter [Melosh, 1989], and the postimpact erosion was about 10 km [Turtle and Pierazzo, 1998]. A simple geometric reconstruction indicates that sites which are currently at distances of 20 km or more from the impact site were at about the same distances during the initial impact event. On the other hand, sites located at shorter distances were displaced significantly with respect to their original locations. We therefore exclude the granite measurement sites at current distances of 15–17 km from the following analysis.

[69] The next stage is to relate the fracture velocity results to the magnitude of the tensile stresses driving the fractures. For this analysis, we assume that the energy density enclosed within the local rock volume is sufficiently large to generate all impact-related fractures at this site. The physical implications of this assumption are as follows:

[70] 1. Any given fracture is “isolated” from its neighboring fractures and the total energy available to drive it is only the energy that is stored within its effective isolated volume. The scale of this effective volume is thus determined by half of the distance between neighboring fractures. A similar assumption has been recently employed in

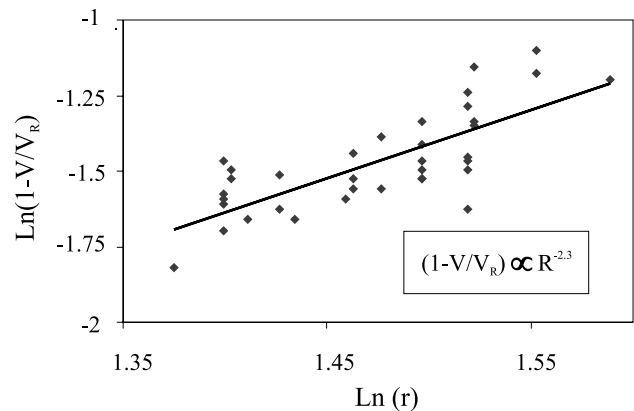


Figure A1. Dependence of $1 - V/V_R$ with the distance, r , from the impact center at Vredefort. Presented values calculated from quartzite, andesite, and chert samples (see text). The values of r were evaluated by assuming 10 km of erosion. The data are consistent with the power law dependence, $(1 - V/V_R) \propto r^{-2.3}$ represented by the solid line.

the analysis of hyperelastic fractures [Buehler *et al.*, 2003].

[71] 2. At any given time, an entire dense ensemble of fractures is propagating at more or less the same velocity.

[72] With these assumptions, we can utilize the equation of motion for a single, rapidly propagating fracture [Freund, 1990] within a “strip” of width b which is loaded with a constant value, σ , of the tensile stress:

$$1 - V/V_R = E\Gamma / (\pi b \pi \sigma^2), \quad (\text{A1})$$

where V is the velocity of the fracture, V_R , E , and Γ are the Rayleigh wave speed, elastic modulus, and fracture energy, respectively (the energy needed to create a unit fracture surface), of the material. Equation (A1) allows us to relate σ to the values of V/V_R derived from our measurements of α , if the mean spacing between fractures, b , can be estimated. Miller *et al.* [1999], in their model of dynamic fragmentation, estimated that:

$$b = 1/n(\sigma)^{1/d}, \quad (\text{A2})$$

where $n(\sigma)$ is the number of activated fractures per unit volume for a given tensile stress, σ , and d is the medium’s dimension [Freund, 1990] ($d = 3$ in the present case); $n(\sigma)$ is taken as the flaw distribution per volume, given by the Weibull distribution [Freund, 1990; Miller *et al.*, 1999]:

$$n(\sigma) = (1/b_w)^d \{(\sigma - \sigma_w)/\sigma_w\}^{m d}. \quad (\text{A3})$$

In equation (A3), b_w is a material-dependent length scale and σ_w is the threshold (Griffith) stress needed to nucleate a fracture; in our case, it is safe to assume that $\sigma \gg \sigma_w$. The parameter m is known as the Weibull exponent and has been empirically found in impact experiments conducted in basalt, sandstone and granodiorite to be in the range $3 < md < 4.2$ [Vardar and Finnie, 1977]. Substitution of equations (A2) and (A3) into equation (A1) yields the

following scaling relation relating the quantity $(1 - V/V_R)$ to the local tensile stress, σ :

$$1 - V/V_R \propto \sigma^{(m-2)}. \quad (\text{A4})$$

We now turn to the dependence of $1 - V/V_R$ with the distance, r , from the impact site at Vredefort. Figure A1 demonstrates that this quantity roughly follows the power law dependence:

$$1 - V/V_R \propto r^{-2.3}. \quad (\text{A5})$$

Substitution of equation (A5) into equation (A4) yields

$$\sigma \propto r^{2.3/(m-2)}, \quad (\text{A6})$$

which thereby predicts a power law decay of the tensile stress, $\sigma \propto r^{-\beta}$. Substitution of the values $1 < m < 1.4$ yields $2.3 < \beta < 3.8$. Previously, power law decay of the shock wave compressive pressure, P , with distance r has been derived by several groups [see Melosh, 1989, chapter 5], which predicted that $P \propto r^{-1.5}$ to $P \propto r^{-4}$. The values predicted by our analysis, $\beta = 2.3-3.8$, are consistent with this 1.5–4.0 range. Our analysis, however, is for tensile stresses, whereas the cited analyses are for the compressive pressure. This similarity of the derived decay rates in the two different analyses leads to a reasonable deduction that the intensity of the tensile stresses generated at the tail of the shock front, may scale with the intensity of the compressive pressure of the front itself. Our estimates of β can be improved with more accurate measurements/estimates of the Weibull exponent.

[73] **Acknowledgments.** We greatly appreciate the fieldwork and discussions with Uwe W. Reimold and Guy E. Charlesworth; the comments and suggestions by Jay Melosh, Gil Cohen, Asenath Wald, Ariel Livne, Shmuel Rubinstein, and Tamir Epstein; and logistic support by Rogers Group's Newton County quarry, Indiana. The careful reviews of Jay Melosh and Tom Ahrens significantly contributed to the quality of the manuscript. The study was supported by the US-Israel BiNational Fund, grant 98-135, and by Israel Science Fund, grant 175-02.

References

- Ahrens, T. J., and A. M. Rubin (1993), Impact-induced tensional failure in rock, *J. Geophys. Res.*, **98**, 1185–1203.
- Albat, H. M. (1988), Shatter cone/bedding interrelationship in the Vredefort structure: Evidence for meteorite impact?, *S. Afr. J. Geol.*, **91**, 106–113.
- Albat, H. M., and J. J. Mayer (1989), Megascopic planar shock fractures in the Vredefort Structure; a potential time marker?, *Tectonophysics*, **162**, 265–276.
- Arakawa, M., K. Shirai, and M. Kato (2000), Shock wave and fracture propagation in water ice by high velocity impact, *Geophys. Res. Lett.*, **27**, 305–308.
- Asphaug, E., J. M. Moore, D. Morrison, W. Benz, M. C. Nolan, and R. J. Sullivan (1996), Mechanical and geological effects of impact cratering on Ida, *Icarus*, **120**, 158–184.
- Bahat, D. (1991), *Tectonofractography*, 354 pp., Springer-Verlag, New York.
- Baratoux, D., and H. J. Melosh (2003), The formation of shatter cones by shock wave interference during impacting, *Earth Planet. Sci. Lett.*, **216**, 43–54.
- Bisschoff, A. A., and J. J. Mayer (1999), Geology of Vredefort Dome, Counc. for Geosci., Pretoria, Republic of South Africa.
- Bouchaud, E., G. Lapasset, and J. Planes (1990), Fractal dimension of fractured surfaces—A universal value, *Europhys. Lett.*, **13**, 73–79.
- Branco, W., and E. Fraas (1905), Das kryptovulkanische Becken von Steinheim, *Phys. Abh. I*, 64 pp., Akad. Wiss., Berlin.
- Buehler, M. J., F. F. Abraham, and H. Gao (2003), Hyperelasticity governs dynamic fracture at a critical length scale, *Nature*, **426**, 141–146.
- Camacho, G. T., and M. Ortiz (1996), Computational modelling of impact damage in brittle materials, *Int. J. Solids Struct.*, **33**, 2899–2938.
- Dietz, R. S. (1947), Meteorite impact suggested by the orientation of shatter-cones at the Kentland, Indiana disturbance, *Science*, **105**, 42–43.
- Dietz, R. S. (1959), Shatter cones in cryptoexplosion structures (meteorite impact?), *J. Geol.*, **67**, 496–505.
- Dietz, R. S. (1963), Cryptoexplosion structures: A discussion, *Am. J. Sci.*, **261**, 650–664.
- Dietz, R. S. (1967), Shatter cone orientation at Gosses Bluff Astrobleme, *Nature*, **216**, 1082–1084.
- Dietz, R. S. (1968), Shatter cones in cryptoexplosion structures, in *Shock Metamorphism of Natural Materials*, edited by B. M. French and N. M. Short, pp. 267–285, Mono Book, Baltimore, Md.
- Dietz, R. S., and L. W. Butler (1964), Shatter-cone orientation at Sudbury Canada, *Nature*, **204**, 280–281.
- Dubuc, B., S. W. Zucker, C. Tricot, J. F. Quiniou, and D. Wehbi (1989), Evaluating the fractal dimension of surfaces, *Proc. R. Soc. London, Ser. A*, **425**, 113–127.
- Evans, A. G., M. E. Gulden, and M. Rosenblatts (1978), Impact damage in brittle materials in the elastic-plastic response regime, *Proc. R. Soc. London, Ser. A*, **361**, 343–365.
- Feder, J. (1988), *Fractals*, 283 pp., Plenum, New York.
- Field, J. E. (1971), Brittle fracture: Its study and application, *Contemp. Phys.*, **12**, 1–31.
- Fineberg, J., and M. Marder (1999), Instability in dynamic fracture, *Phys. Rep.*, **313**, 2–108.
- French, B. M. (1998), *Traces of Catastrophe. Handbook of Shock-Metamorphic Effects in Terrestrial Meteorite Impact Structures*, 120 pp., Lunar and Planet. Inst., Houston, Tex.
- Freund, L. B. (1990), *Dynamic Fracture Mechanics*, 563 pp., Cambridge Univ. Press, New York.
- Fuller, K. N. G., P. G. Fox, and J. E. Field (1975), Temperature rise at tip of fast-moving cracks in glassy polymers, *Proc. R. Soc. London, Ser. A*, **341**, 537–557.
- Gash, P. J. S. (1971), Dynamic mechanism for the formation of shatter cones, *Nature*, **230**, 32–35.
- Gay, N. C. (1976), Spherules on shatter cone surfaces from Vredefort structure, South-Africa, *Science*, **194**, 724–725.
- Gibson, R. L., W. U. Reimold, and G. Stevens (1998), Thermal-metamorphic signature of an impact event in the Vredefort dome, South Africa, *Geology*, **26**, 787–790.
- Grieve, R. A. F., and L. J. Pesonen (1992), The terrestrial impact cratering record, *Tectonophysics*, **216**, 1–30.
- Gutschick, R. C. (1976), Geology of the Kentland structural anomaly, northwestern Indiana, paper presented at Geological Society of America Annual Meeting, North-Central Section, Kalamazoo, Mich.
- Gutschick, R. C. (1983), Geology of the Kentland Dome structurally complex anomaly, northwestern Indiana, in *Field Trips in Midwestern Geology*, edited by R. H. Shaver and J. A. Sunderman, pp. 105–138, Geol. Soc. of Am., Boulder, Colo.
- Halls, H. C., and R. A. F. Grieve (1976), Slate Islands—Probable complex meteorite impact structure in Lake Superior, *Can. J. Earth Sci.*, **13**, 1301–1309.
- Hansen, A., E. L. Hinrichsen, and S. Roux (1991), Roughness of crack interfaces, *Phys. Rev. Lett.*, **66**, 2476–2479.
- Hargraves, R. B. (1961), Shatter cones in the rocks of the Vredefort ring, *Trans. Geol. Soc. S. Afr.*, **64**, 147–154.
- Henkel, H., and W. U. Reimold (1998), Integrated geophysical modelling of a giant, complex impact structure: anatomy of the Vredefort structure, South Africa, *Tectonophysics*, **287**, 1–20.
- Howard, K. A., and T. W. Offield (1968), Shatter cones at Sierra Madera Texas, *Science*, **162**, 261–265.
- Johnson, G. P., and R. J. Talbot (1964), A theoretical study of the shock wave origin of shatter cones, M.Sc. thesis, Air Force Inst. of Technol., Dayton, Ohio.
- Kamo, S. L., W. U. Reimold, T. E. Krogh, and W. P. Colliston (1996), A 2.023 Ga age for the Vredefort impact event and a first report of shock metamorphosed zircons in pseudotachylitic breccias and Granophyre, *Earth Planet. Sci. Lett.*, **144**, 369–387.
- Laney, R. T., and W. R. Van Schmus (1978), A structural study of the Kentland, Indiana impact site, *Proc. Lunar Planet. Sci. Conf.*, **9th**, 2609–2632.
- Maloy, K. J., A. Hansen, E. L. Hinrichsen, and S. Roux (1992), Experimental measurements of the roughness of brittle cracks, *Phys. Rev. Lett.*, **68**, 213–215.
- Manton, W. I. (1965), The orientation and origin of shatter cones in the Vredefort ring, *Ann. N. Y. Acad. Sci.*, **123**, 1017–1049.

- Martini, J. E. J. (1978), Coesite and stishovite in Vredefort Dome, South Africa, *Nature*, *272*, 715–717.
- Melosh, H. J. (1989), *Impact Cratering: A Geologic Process*, 245 pp., Oxford Univ. Press, New York.
- Melosh, H. J., E. V. Ryan, and E. Asphaug (1992), Dynamic fragmentation in impacts: Hydrocode simulation of laboratory impacts, *J. Geophys. Res.*, *97*, 14,735–14,759.
- Miller, O., L. B. Freund, and A. Needleman (1999), Modeling and simulation of dynamic fragmentation in brittle materials, *Int. J. Fract.*, *96*, 101–125.
- Milton, D. J. (1977), Shatter cones—An outstanding problem in shock mechanics, in *Impact and Explosion Cratering: Planetary and Terrestrial Implications*, edited by D. J. Roddy, R. O. Pepin, and R. B. Merrill, pp. 703–714, Pergamon, New York.
- Morrissey, J. W., and J. R. Rice (1998), Crack front waves, *J. Mech. Phys. Solids*, *46*, 467–487.
- Morrissey, J. W., and J. R. Rice (2000), Perturbative simulations of crack front waves, *J. Mech. Phys. Solids*, *48*, 1229–1251.
- Nicolaysen, L. O., and W. U. Reimold (1999), Vredefort shatter cones revisited, *J. Geophys. Res.*, *104*, 4911–4930.
- O'Keefe, J. D., and T. J. Ahrens (1993), Planetary cratering mechanics, *J. Geophys. Res.*, *98*, 17,011–17,028.
- Ramanathan, S., and D. S. Fisher (1997), Dynamics and instabilities of planar tensile cracks in heterogeneous media, *Phys. Rev. Lett.*, *79*, 877–880.
- Reimold, W. U., and R. L. Gibson (1996), Geology and evolution of the Vredefort impact structure, South Africa, *J. Afr. Earth Sci.*, *23*, 125–162.
- Reimold, W. U., M. Andreoli, and R. J. Hart (1985), A geochemical study on pseudotachylite and parent rocks from the Vredefort structure, *Meteoritics*, *20*, 740–742.
- Repetto, E. A., R. Radovitzky, and M. Ortiz (2000), Finite element simulation of dynamic fracture and fragmentation of glass rods, *Comput. Method. Appl. Mech.*, *183*, 3–14.
- Riou, P., C. E. Cottenot, and M. Boussuge (1998), Anisotropic damage model for impacted ceramic material: Application to silicon carbide, *Int. J. Impact Eng.*, *21*, 683–693.
- Roach, D. E., A. D. Fowler, and W. K. Fyson (1993), Fractal fingerprinting of joint and shatter-cone surfaces, *Geology*, *21*, 759–762.
- Roddy, D. J., and L. K. Davis (1977), Shatter cones formed in large scale experimental explosion craters, in *Impact and Explosion Cratering: Planetary and Terrestrial Implications*, edited by D. J. Roddy, R. O. Pepin, and R. B. Merrill, pp. 715–750, Pergamon, New York.
- Sagy, A., Z. Reches, and I. Roman (2001), Dynamic fracturing; field and experimental observations, *J. Struct. Geol.*, *23*, 1223–1239.
- Sagy, A., Z. Reches, and J. Fineberg (2002), Dynamic fracture by large extraterrestrial impacts as the origin of shatter cones, *Nature*, *418*, 310–313.
- Schneider, E., and G. A. Wagner (1976), Shatter cones produced experimentally by impacts in limestone targets, *Earth Planet. Sci. Lett.*, *32*, 40–44.
- Sharon, E., and J. Fineberg (1996), Microbranching instability and the dynamic fracture of brittle materials, *Phys. Rev.*, *54*, 7128–7139.
- Sharon, E., S. P. Gross, and J. Fineberg (1995), Local crack branching as a mechanism for instability in dynamic fracture, *Phys. Rev. Lett.*, *74*, 5096–5099.
- Sharon, E., G. Cohen, and J. Fineberg (2001), Propagating solitary waves along a rapidly moving crack front, *Nature*, *410*, 68–71.
- Sharon, E., G. Cohen, and J. Fineberg (2002), Crack front waves and the dynamics of a rapidly moving crack, *Phys. Rev. Lett.*, *88*, article 085503.
- Sharpton, V. L., B. O. Dressler, R. R. Herrick, B. Schnieders, and J. Scott (1996), New constraints on the Slate Islands impact structure, Ontario, Canada, *Geology*, *24*, 851–854.
- Shrock, R. R. (1937), Stratigraphy and structure of the area of disturbed Ordovician rocks near Kentland, Indiana, *Am. Midlands Nat.*, *18*, 471–531.
- Simha, C. H. M., S. J. Bless, and A. Bedford (2002), Computational modeling of the penetration response of a high-purity ceramic, *Int. J. Impact Eng.*, *27*, 65–86.
- Stesky, R. M., and H. C. Halls (1983), Structural analysis of shatter cones from the Slate Islands, northern Lake Superior, *Can. J. Earth Sci.*, *20*, 1–18.
- Therriault, A. M., R. A. F. Grieve, and W. U. Reimold (1997), Original size of the Vredefort structure: Implications for the geological evolution of the Witwatersrand basin, *Meteorit. Planet. Sci.*, *32*, 71–77.
- Tudor, D. S. (1971), A geophysical study of the Kentland disturbed area, Ph.D. thesis, 111 pp., Indiana Univ., Bloomington.
- Turtle, E. P., and E. Pierazzo (1998), Constraints on the size of the Vredefort impact crater from numerical modeling, *Meteorit. Planet. Sci.*, *33*, 483–490.
- Vardar, O., and I. Finnie (1977), Prediction of fracture in brittle solids subjected to very short duration tensile stresses, *Int. J. Fract.*, *13*, 115–131.
- Yoffe, E. H. (1951), The moving Griffith crack, *Philos. Mag.*, *42*, 739–750.

A. Sagy and Z. Reches, Institute of Earth Sciences, Hebrew University of Jerusalem, 91904 Jerusalem, Israel. (sagy@vms.huji.ac.il; reches@earth.es.huji.ac.il)

J. Fineberg, Racah Institute of Physics, Hebrew University of Jerusalem, 91904 Jerusalem, Israel. (jay@vms.huji.ac.il)